

<sup>1</sup> **Whole-brain comparison of rodent and human brains  
using spatial transcriptomics**

<sup>3</sup>

<sup>4</sup> Antoine Beauchamp<sup>1,2,3,\*</sup>, Yohan Yee<sup>1,2,3</sup>, Ben C. Darwin<sup>1,2</sup>, Armin Raznahan<sup>4</sup>, Rogier B.  
<sup>5</sup> Mars<sup>5,6,†</sup>, Jason P. Lerch<sup>1,2,3,5,\*†</sup>

<sup>6</sup>

<sup>7</sup> <sup>1</sup>Mouse Imaging Centre, Toronto, Ontario, Canada.

<sup>8</sup> <sup>2</sup>The Hospital for Sick Children, Toronto, Ontario, Canada.

<sup>9</sup> <sup>3</sup>Department of Medical Biophysics, University of Toronto, Toronto, Ontario, Canada.

<sup>10</sup> <sup>4</sup>Section on Developmental Neurogenomics, Human Genetics Branch, National Institute of Mental Health Intramural  
<sup>11</sup> Research Program, Bethesda, MD, U.S.A.

<sup>12</sup> <sup>5</sup>Wellcome Centre for Integrative Neuroimaging, Centre for Functional MRI of the Brain (FMRIB), Nuffield Depart-  
<sup>13</sup> ment of Clinical Neurosciences, John Radcliffe Hospital, University of Oxford, Oxford, United Kingdom.

<sup>14</sup> <sup>6</sup>Donders Institute for Brain, Cognition and Behaviour, Radboud University Nijmegen, Nijmegen, Netherlands.

<sup>15</sup> <sup>†</sup>These authors contributed equally to this work.

<sup>16</sup> \*Corresponding author. Email: antoine.beauchamp@mail.utoronto.ca (A.B.); jason.lerch@ndcn.ox.ac.uk (J.P.L)

<sup>17</sup> **Abstract**

<sup>18</sup> The ever-increasing use of mouse models in preclinical neuroscience research calls for an improvement in the  
<sup>19</sup> methods used to translate findings between mouse and human brains. Previously we showed that the brains  
<sup>20</sup> of primates can be compared in a direct quantitative manner using a common reference space built from  
<sup>21</sup> white matter tractography data (Rogier B. Mars et al., 2018b). Here we extend the common space approach  
<sup>22</sup> to evaluate the similarity of mouse and human brain regions using openly accessible brain-wide transcrip-  
<sup>23</sup> tomic data sets. We show that mouse-human homologous genes capture broad patterns of neuroanatomical  
<sup>24</sup> organization, but that the resolution of cross-species correspondences can be improved using a novel su-  
<sup>25</sup> pervised machine learning approach. Using this method, we demonstrate that sensorimotor subdivisions of  
<sup>26</sup> the neocortex exhibit greater similarity between species, compared with supramodal subdivisions, and that  
<sup>27</sup> mouse isocortical regions separate into sensorimotor and supramodal clusters based on their similarity to  
<sup>28</sup> human cortical regions. We also find that mouse and human striatal regions are strongly conserved, with  
<sup>29</sup> the mouse caudoputamen exhibiting an equal degree of similarity to both the human caudate and putamen.

## 30 Introduction

31 Animal models play an indispensable role in neuroscience research, not only for understanding disease and  
32 developing treatments, but also for obtaining data that cannot be obtained in the human. While numerous  
33 species have been used to model the human brain, the mouse has emerged as the most prominent of these,  
34 due to its rapid life cycle, straightforward husbandry, and amenability to genetic engineering (Dietrich et  
35 al., 2014; Ellenbroek and Youn, 2016; Hedrich et al., 2004; Houdebine, 2004). Mouse models have proven  
36 to be extremely useful for understanding diverse features of the brain, from its molecular neurobiological  
37 properties to its large-scale network properties (Hodge et al., 2019; Oh et al., 2014; Yao et al., 2021).  
38 However, translating findings from the mouse to the human has not been straightforward. This is especially  
39 evident in the context of neuropsychopharmacology, where promising neuropsychiatric drugs have one of the  
40 highest failures rates in Phase III clinical trials (Hay et al., 2014).

41 Successful translation requires an understanding of how effects on the brain of the model species are likely to  
42 manifest in the brain of the actual species of interest. This is not trivial in the case of the mouse and human,  
43 as the two species diverged from a common ancestor about 80 million years ago (Kaas, 2012). Although  
44 common themes are apparent in the brains of all mammalian species studied to date (Krubitzer, 2007), there  
45 remain substantial differences between the mouse and human brain. Beyond the obvious differences in size,  
46 large parts of the human cortex potentially have no corresponding homologues in the mouse (Preuss, 1995).  
47 Direct comparisons across the brains of different species are further complicated by the fact that researchers  
48 from different traditions use inconsistent nomenclature to refer to similar neuroanatomical areas (Heukelum  
49 et al., 2020; Laubach et al., 2018).

50 Over the course of the last decade, we have developed novel approaches to explicitly evaluate similarities  
51 and differences between the brains of related species. These approaches describe brains using common data  
52 spaces that are directly comparable between species, making it possible to evaluate the similarity of different  
53 regions in a quantitative fashion (Mars et al., 2021). This way, potential homologues can be formally tested  
54 and regions of the brain that do not allow for straightforward translation can be identified (Rogier B. Mars  
55 et al., 2018b). Establishing such a formal translation between the mouse and the human brain would allow  
56 scientists involved in translational research to explicitly test hypotheses about conservation of brain regions,  
57 identify regions that are well suited to translational paradigms, and directly transform quantitative maps  
58 from the brain of one species to the other.

59 One approach towards building these common spaces has been to exploit connectivity. It has previously  
60 been demonstrated that brain regions can be identified via their unique set of connections to other regions

in the brain. This *connectivity fingerprint* can therefore be seen as a diagnostic of an area (Rogier B. Mars et al., 2018a; Passingham et al., 2002). The common connectivity space approach relies on defining agreed upon neuroanatomical homologues *a priori* and then expressing the connectivity fingerprint of regions under investigation with those established homologues in the two brains (Mars et al., 2016b). The connections of any given region to the established homologues thus form a common space, which links the two brains. In a series of early studies, we compared the connectivity of the macaque and human brain, identifying homologies as well as specializations across association cortex (Mars et al., 2013; Neubert et al., 2014; Sallet et al., 2013). The same approach has recently been applied to mouse-human comparisons for the first time, demonstrating conserved organization between the mouse and human striatum, but some specialization in the human caudate related to connectivity with the prefrontal cortex (Balsters et al., 2020). A similar study recently compared connectivity of the medial frontal cortex across rats, marmosets, and humans (Schaeffer et al., 2020). However, the lack of established neuroanatomical homologues in mice, particularly in the cortex, limits the use of connectivity to compare these species.

A more promising approach to mouse-human comparisons could be to exploit the spatial patterns of gene expression. Advances in transcriptomic mapping can be used to characterise the differential expression of many thousands of genes across the brain and compare the pattern between regions (Ortiz et al., 2020). Moreover, the availability of whole-brain spatial transcriptomic data sets for multiple species provides an opportunity to run novel analyses at low cost (Hawrylycz et al., 2012; Lein et al., 2007). Such maps for the human cortex show topographic patterns that mimic those observed in other modalities, such as a gradient between primary and heteromodal areas of the neocortex (Burt et al., 2018). Importantly, these patterns appear to be conserved across mammalian species (Fulcher et al., 2019), which opens up the possibility of using the expression of homologous genes as a common space across species. In fact, a recent study demonstrated how the expression of homologous genes can be used to directly register mouse and vole brains into a common reference frame, which allows for direct point-xby-point comparisons of brain maps (Englund et al., 2021). However, this specific approach is only feasible because of the large degree of morphological similarity between mouse and vole brains. In the case of mouse-human comparisons, we almost certainly cannot directly register mouse and human brains into a common coordinate frame using methods for image registration. Hence we need to be more creative in our approach.

Here we examine the patterns of similarity between the mouse and human brain using a common space constructed from spatial gene expression data sets. We begin with an initial set of 2835 homologous genes. Subsequently, we present and evaluate a novel method for improving the resolution of mouse-human neuroanatomical correspondences using a supervised machine learning approach. Using the novel representation

93 of the gene expression common space, i.e. a latent gene expression space, we analyse the similarity of mouse  
94 and human isocortical subdivisions and demonstrate that sensorimotor regions exhibit a higher degree of sim-  
95 ilarity than supramodal regions. Finally, we examine the patterns of transcriptomic similarity at a voxel-wise  
96 level in the mouse and human striatum.

## 97 Results

### 98 Homologous genes capture broad similarities in the mouse and human brains

99 We first examined the pattern of similarities that emerged when comparing mouse and human brain regions  
100 on the basis of their gene expression profiles. We constructed a gene expression common space using widely  
101 available data sets from the Allen Institute for Brain Science: the Allen Mouse Brain Atlas (AMBA) and  
102 the Allen Human Brain Atlas (AHBA) (Hawrylycz et al., 2012; Lein et al., 2007). These data sets provide  
103 whole-brain coverage of expression intensity for thousands of genes in the mouse and human genomes. For  
104 our purposes we filtered these gene sets to retain only mouse-human homologous genes using a list of ortho-  
105 logues obtained from the NCBI HomoloGene system (NCBI 2018). Using a gene enrichment analysis, we  
106 found that this reduced gene set was significantly associated with a number of biological processes related to  
107 the nervous system, with Gene Ontology labels such as “nervous system development”, “neurogenesis”, and  
108 “regulation of nervous system development”. Additional modules returned with high significance were “reg-  
109 ulation of multicellular organismal process”, “regulation of biological quality”, and “multicellular organism  
110 development”. The full set of significant modules can be found in Supplementary File 1.

111 Prior to analysis, the mouse and human homologous gene expression data sets were pre-processed using a  
112 pipeline that included quality control checks, normalization procedures, and aggregation of the expression  
113 values under a set of atlas labels. The result was a gene-by-region matrix in either species, describing the  
114 normalized expression of 2835 homologous genes across 67 mouse regions and 88 human regions (see Materials  
115 and methods). We quantified the degree of similarity between all pairs of mouse and human regions using  
116 the Pearson correlation coefficient, resulting in a mouse-human similarity matrix (Figure 1A).

117 We find that the similarity matrix exhibits broad patterns of positive correlation between the mouse and  
118 human brains. These clusters of similarity correspond to coarse neuroanatomical regions that are generally  
119 well-defined in both species. For instance, we observe that, overall, the mouse isocortex is similar to the  
120 human cerebral cortex, with the exception of the hippocampal formation, which forms a unique cluster.  
121 Similarly the mouse and human cerebellar hemispheres cluster together, while the cerebellar nuclei show

122 relatively high correlation to each other ( $r = 0.404$ ) as well as to brain stem structures like the pons ( $r = 0.359$   
123 and  $r = 0.371$  for the mouse and human nuclei respectively) and myelencephalon ( $r = 0.318$  and  $r = 0.374$ ).  
124 The associations between broad regions such as these are self-evident in the correlation matrix.  
  
125 Our ability to resolve regional matches on a finer scale is limited when using all homologous genes in this way.  
126 This is especially true for regions within the cerebral and cerebellar cortices, which exhibit a high degree  
127 of internal homogeneity. This is apparent in the similarity profiles, defined here as the set of correlation  
128 values between a given seed region and all target regions in the other species. For example, the human  
129 precentral gyrus and cuneus are most strongly correlated to many regions of the mouse isocortex. While  
130 the brain maps feature a rostral-caudal gradient (Figure 1B), the profiles of the two seeds are highly similar  
131 despite the regions having very different functions (Figure 1C). Indeed, the correlation between the similarity  
132 profiles of the precentral gyrus and cuneus is  $r = 0.980$ . The similarity profile of human cerebellar crus 1  
133 highlights another example of this homogeneity. The profile of crus 1 is similar to that of all regions of the  
134 mouse cerebellum, with an average correlation of  $r = 0.269$  and a standard deviation of  $\sigma = 0.041$ . Across  
135 all regions, the variance of the correlations across cortical regions is  $\sigma^2 = 0.0052$  while that across cerebellar  
136 hemispheric regions is  $\sigma^2 = 0.0017$ , compared with a total variation of  $\sigma^2 = 0.0416$  across all entries in the  
137 matrix.  
  
138 So, although there is some distinguishing power in the profiles of regions at a finer scale, this is much smaller  
139 than between coarse anatomical regions. This is also true for parts of the broad anatomical systems that are  
140 part of the same functional system. This suggests that the regional expression patterns of mouse-human  
141 homologous genes can be used to identify general similarities between the brains of the two species even  
142 using a simple correlation measure, but the ability to identify finer scale matches might require a more  
143 subtle approach.

144 **A latent gene expression space improves the resolution of mouse-human associations**  
145

146 In the previous analyses, we showed that the expression profiles of homologous genes capture broad simi-  
147 larities across the mouse and the human for the major subdivisions of the brain. Some information at a  
148 finer resolution (e.g. within the isocortex) was also evident, but much less distinctive. Our next goal was  
149 to investigate whether it is possible to leverage the gene expression data sets to relate mouse and human  
150 brains to one another at a finer regional level. In order to do so, we sought to maximise the informational  
151 value in the set of 2835 homologous genes by creating a new latent common space that exploits the regional

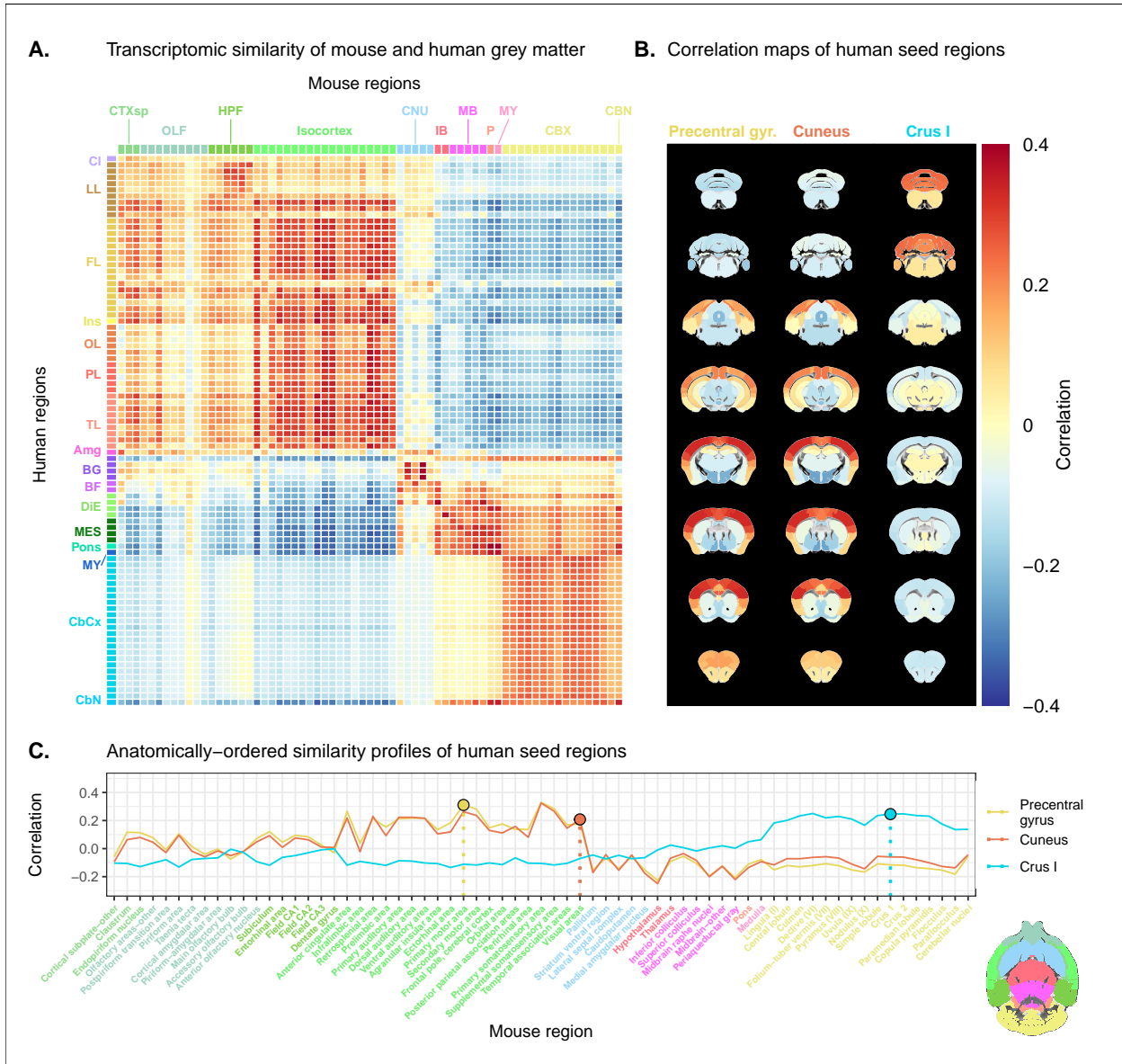


**Figure 1.** Transcriptomic similarity in the mouse and human brains. **(A)** Similarity matrix displaying the correlation between 67 mouse regions and 88 human regions based on the expression of 2835 homologous genes. Columns are annotated with 11 broad mouse regions: Cortical subplate (CTXsp), olfactory areas (OLF), hippocampal formation (HPF), isocortex, cerebral nuclei (CNU), interbrain (IB), midbrain (MB), pons (P), medulla (MY), cerebellar cortex (CBX), cerebellar nuclei (CBN). Rows are annotated with 16 broad human regions: Claustrum (CL), limbic lobe (LL), frontal lobe (FL), insula (Ins), occipital lobe (OL), parietal lobe (PL), temporal lobe (TL), amygdala (Amg), basal ganglia (BG), basal forebrain (BF), diencephalon (DIE), mesencephalon (MES), pons, myelencephalon (MY), cerebellar cortex (CbCx), cerebellar nuclei (CbN). Broad patterns of similarity are evident between coarsely defined brain regions, while correlation patterns are mostly homogeneous within these regions. **(B)** Mouse brain coronal slices showing similarity profiles for the human precentral gyrus, cuneus and crus I. Correlation patterns for the precentral gyrus and cuneus are highly similar to one another and broadly similar to most isocortical regions. The crus I is homogeneously similar to the mouse cerebellum. **(C)** Anatomically-ordered line charts displaying the similarity profiles for the seed regions in (B). Dashed vertical lines indicate the canonical mouse homologue for each human seed. Annotation colours correspond to atlas colours from the AMBA and AHBA for mouse and human regions respectively.

152 distinctiveness of the expression profiles.

153 The approach used in the previous analysis relied on using homologous genes as a common space between  
154 the mouse and human brain. This approach effectively assigns equal value to each gene, whereas a more  
155 powerful approach would be to weight genes by their ability to distinguish between different brain regions.  
156 We investigated whether we could accomplish this by constructing a new set of variables from combinations  
157 of the homologous genes. Our primary goal here was to transform the initial gene space into a new common  
158 space that would improve the locality of the matches. However while we sought a transformation that would  
159 allow us to recapitulate known mouse-human neuroanatomical homologues, we also wanted to avoid directly  
160 encoding such correspondences in the transformation. Using this information as part of the optimization  
161 process for the transformation would run the risk of driving the transformation towards mouse-human pairs  
162 that are already known. While we are interested in being able to recover such matches, we are equally  
163 interested in identifying novel and unexpected associations between neuroanatomical regions in the mouse  
164 and human brains (e.g. one-to-many correspondences). Given these criteria, our approach to identifying an  
165 appropriate transformation was to train a multi-layer perceptron classifier on the data from the AMBA. The  
166 classifier was tasked with predicting the 67 labels in our mouse atlas from the voxel-wise expression of the  
167 homologous genes (Figure 2A).

168 While the model could have been trained using the data from either species, we chose to use the mouse  
169 data because it provides continuous coverage of the entire brain and is thus better suited to this purpose.  
170 In training the model to perform this classification task, we effectively optimize the network architecture  
171 to identify a transformation from the input gene space to a space that encodes information about the  
172 delineation between mouse brain regions. To extract this transformation, we removed the output layer from  
173 the trained neural network. The resulting architecture defines a transformation from the input space to  
174 a lower-dimensional gene expression latent space. We then applied this transformation to the mouse and  
175 human gene-by-region expression matrices to obtain representations of the data in the latent common space  
176 (Figure 2B). Finally, we used these gene expression latent common space matrices to compute the new  
177 similarity matrix (Figure 2C). Since the optimization algorithm used to train the perceptron features an  
178 inherent degree of stochasticity, we repeated this training and transformation process 500 times to generate  
179 a distribution of latent spaces and similarity matrices over training runs. Although the neural network and  
180 associated latent space do not directly provide information about which genes are most important for the  
181 classification of specific mouse atlas labels, this type of information can be derived from the model using  
182 attribution methods such as integrated gradients (Figure 2-figure supplement 1) (Sundararajan et al., 2017).  
183 Each brain region in the classification task is associated with the input genes in different ways, such that

184 there isn't a single weighting of gene importance for the entire model. While most genes contribute to the  
 185 classification of any given label in some capacity, it is often the case that the network relies on a reduced  
 186 subset of genes to arrive at a decision. For example, the genes *Prrg2* and *Rgs2* were found to be most  
 187 influential for the classification of the caudoputamen, when the feature attributions were averaged over all  
 188 training runs. In contrast, *Rfx4* and *Tnncl* were the most influential for the classification of the primary  
 189 motor area. In some cases, the spatial expression pattern of the gene clearly shows a demarcation of the  
 190 region of interest (e.g. *Rgs2*), but this is not always the case, nor is it necessary, as the network learns from  
 191 the entire gene expression signature of all voxels.

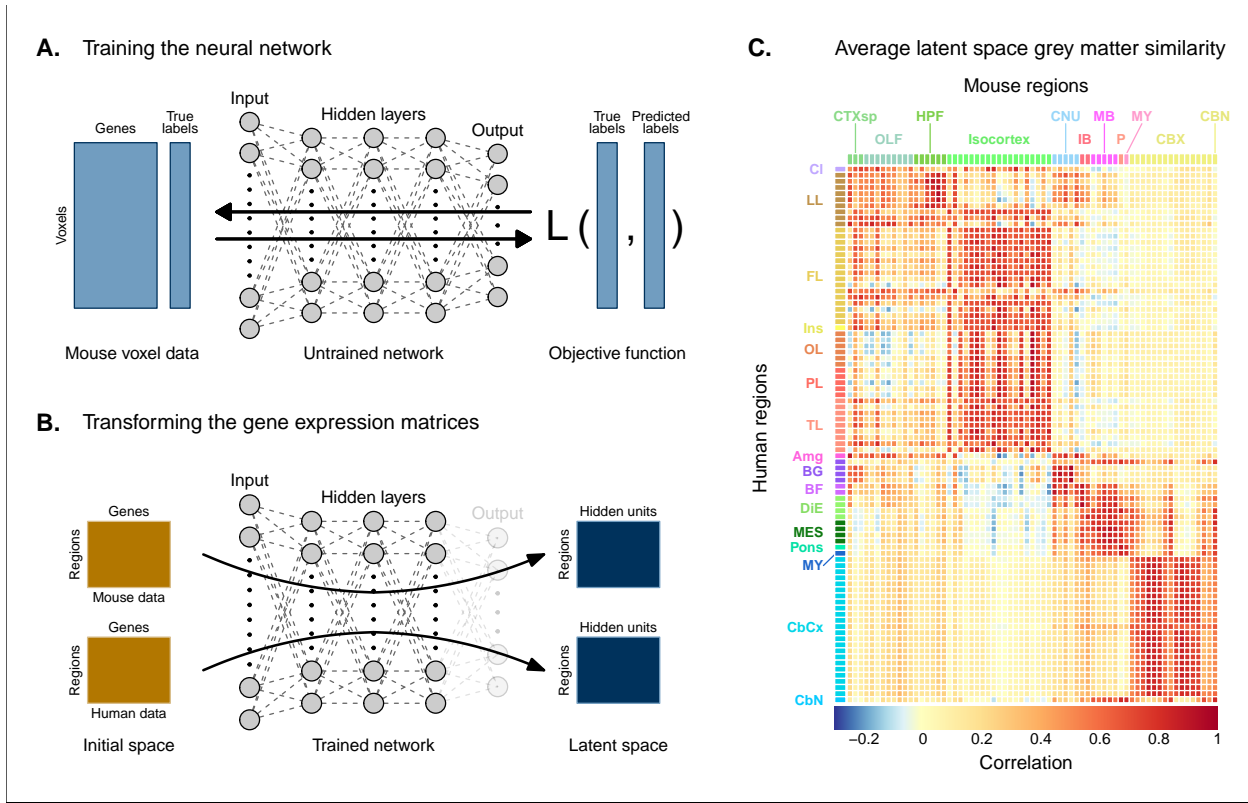


**Figure 2.** Creating a new common space. **(A)** Voxel-wise expression maps from 2835 homologous genes in the AMBA were used to train the neural network to classify each mouse voxel into one of 67 atlas regions. **(B)** Once the network is trained, the output layer is removed. The mouse and human regional gene expression matrices are passed through the network, resulting in lower-dimensional latent space representations of the data. The training and transformation process was repeated 500 times. **(C)** A similarity matrix displaying the gene expression latent space correlation between mouse and human regions, averaged over 500 neural network training runs. Similar brain regions exhibit very high correlation values. Column and row annotations as described in Figure 1.

192 To assess whether the latent space representations of the data improved the resolution of the mouse-human  
 193 matches, we considered two criteria. The first was whether the similarity profiles of the mouse atlas regions  
 194 were more localized within the corresponding broad regions of interest (e.g. primary motor area within  
 195 isocortex), compared with their similarity profiles in the original gene space. We term this the locality  
 196 criterion. The second criterion was whether the degree of similarity between canonical neuroanatomical  
 197 homologues improved in this new latent common space. We term this the homology criterion. The locality

198 criterion tells us about our ability to extract finer-scale signal in these profiles, while the homology criterion  
199 informs us about our ability to recover expected matches in this finer-scale signal. To evaluate these criteria,  
200 we computed ranked similarity profiles for every region in the mouse brain, ordered such that a rank of 1  
201 indicates the most similar human region. In addition, given the difference in absolute value between the  
202 input gene space and gene expression latent space correlations, we scaled the similarity profiles to the interval  
203 [0, 1] in order to make comparisons between the spaces.

204 We evaluated the locality criterion by examining the decay rate of the top of the similarity profiles. We  
205 reasoned that the plateau of similarity to a broad brain region, as seen in the anatomically-ordered similarity  
206 matrices and profiles (Figure 1, A and C; Figure 2C), would correspond to a similar plateau at the head of  
207 the rank-ordered profiles. Moreover, the emergence of local signal would manifest as an increase in the range  
208 between the peaks and troughs within the broad region. In the rank-ordered profiles, this would correspond  
209 to a faster rate of decay at the head of the profile. In order to quantify this decay, we computed the rank  
210 at which each region's similarity profile decreased to a scaled value of 0.75. This was calculated for every  
211 mouse region in the initial gene space, as well as in each of the 500 gene expression latent spaces. As a  
212 measurement of performance between the two representations of the data, we then took the difference in this  
213 rank between each of the latent spaces and the original gene space (Figure 3A). A negative rank difference  
214 indicates an improvement in the latent space.

215 Examining the structure-wise distributions of these rank differences, we found that for the majority of regions  
216 in our mouse atlas, the classification approach resulted in either an improvement in the amount of locality  
217 within a broad region, or no difference from the original gene space (Figure 3, B and C). We quantified the  
218 improvement overall by fitting a logistic regression model with no predictors to the mean rank differences  
219 of each of the atlas regions. We considered the success condition for the Bernoulli trials to be a mean rank  
220 difference less than or equal to zero. The model estimate for the Bernoulli probability was  $p = 0.78$  with a  
221 95% confidence interval of [0.66, 0.86]. In other words, 52 of the 67 brain regions saw an improvement on  
222 average when using the latent spaces. We additionally evaluated the same kind of logistic regression on a  
223 region-wise basis to quantify how often the latent spaces resulted in an improvement for individual brain  
224 regions (Figure 3C). We found that for 49 regions (73%), the model estimated the probability to be at least  
225 at high as  $p = 0.95$ . While confidence intervals varied around this estimate, the range between the upper  
226 and lower bound was only ever as high as 0.04. Thus these estimates are much higher than the expected  
227 null probability of  $p = 0.50$ . A few regions performed worse in the latent spaces, notably the dentate gyrus  
228 ( $p = 0.0$ , no variance), the thalamus ( $p = 0.0020$ , 95% CI [0.0003, 0.0146]), and the lateral septal complex  
229 ( $p = 0.004$ , 95% CI [0.001, 0.016]). Beyond this binary measure of improvement, some regions exhibited a

230 large range of differences in rank over the various latent spaces. In particular regions like the main olfactory  
231 bulb (mean rank difference of  $\mu = 7$ , 95% CI  $[-12, 27]$ ) and accessory olfactory bulb  $\mu = -3$ , 95% CI  
232  $[-27, 22]$ ) exhibit a substantial degree of variance. Other than these two areas, regions within the olfactory  
233 areas (e.g. piriform area) were among those that benefited the most from the classification approach, showing  
234 improvement in all sampled latent spaces. While the effects, i.e. rank differences, are smaller, the similarity  
235 profiles of regions belonging to the isocortex and cerebellar cortex also saw an improvement in locality. All  
236 models for isocortical areas returned probability estimates greater than  $p = 0.95$ . Moreover, 13 of the 19  
237 isocortical regions were improved in all latent spaces. Brain regions belonging to the cerebellar cortex saw  
238 similar improvement. In contrast, regions belonging to the cerebral nuclei, the diencephalon, midbrain and  
239 hindbrain did not see much improvement in this new common space, with an average probability estimate of  
240  $p = 0.36$  for this subset. For many such regions the degree of locality appears to be worse in this space, though  
241 only by a small number of ranks, e.g. striatum ventral region (mean rank difference of  $\mu = 2$ , 95% CI  $[-1, 5]$ )  
242 and lateral septal complex ( $\mu = 6$ , 95% CI  $[2, 10]$ ). Indeed, computing the average rank difference over this  
243 subset of regions across all latent spaces, we find  $\mu = 2$  with 95% confidence interval  $[-3, 6]$ . These results  
244 demonstrate that the supervised learning approach used here can improve the resolution of neuroanatomical  
245 correspondences between the mouse and human brains, though the amount of improvement varies over the  
246 brain. Regions that were already well-characterized using the initial set of homologous genes (e.g. subcortical  
247 regions) did not benefit tremendously, but numerous regions in the cortical plate and subplate, as well as  
248 the cerebellum, saw an improvement in locality in this new common space.

249 While the supervised learning approach improved our ability to identify matches on a finer scale for a number  
250 of brain regions, this does not necessarily mean that those improved matches are biologically meaningful. The  
251 second criterion for evaluating the performance of the neural network addresses whether this improvement  
252 in locality captures what we would expect in terms of known mouse-human homologies. To this end, we  
253 examined the degree of similarity between established mouse-human neuroanatomical pairs, both in the  
254 initial gene expression space and in the set of latent spaces. We began by establishing a list of 36 canonical  
255 mouse-human homologous pairs on the basis of common neuroanatomical labels in our atlases. For each of  
256 these regions in the mouse brain, we compared the rank of the canonical human match in the rank-ordered  
257 similarity profiles between the latent spaces and the original gene expression space (Figure 4A). The lower  
258 the rank, the more similar the canonical pair, with a rank of 1 indicating maximal similarity. As described  
259 above, we evaluated the overall performance of the classification approach by running a logistic regression  
260 using the average latent space rank difference over all regions in our subset. Here we find an estimated  
261 probability of  $p = 0.58$  with 95% confidence interval  $[0.42, 0.73]$ . This is consistent with the null hypothetical

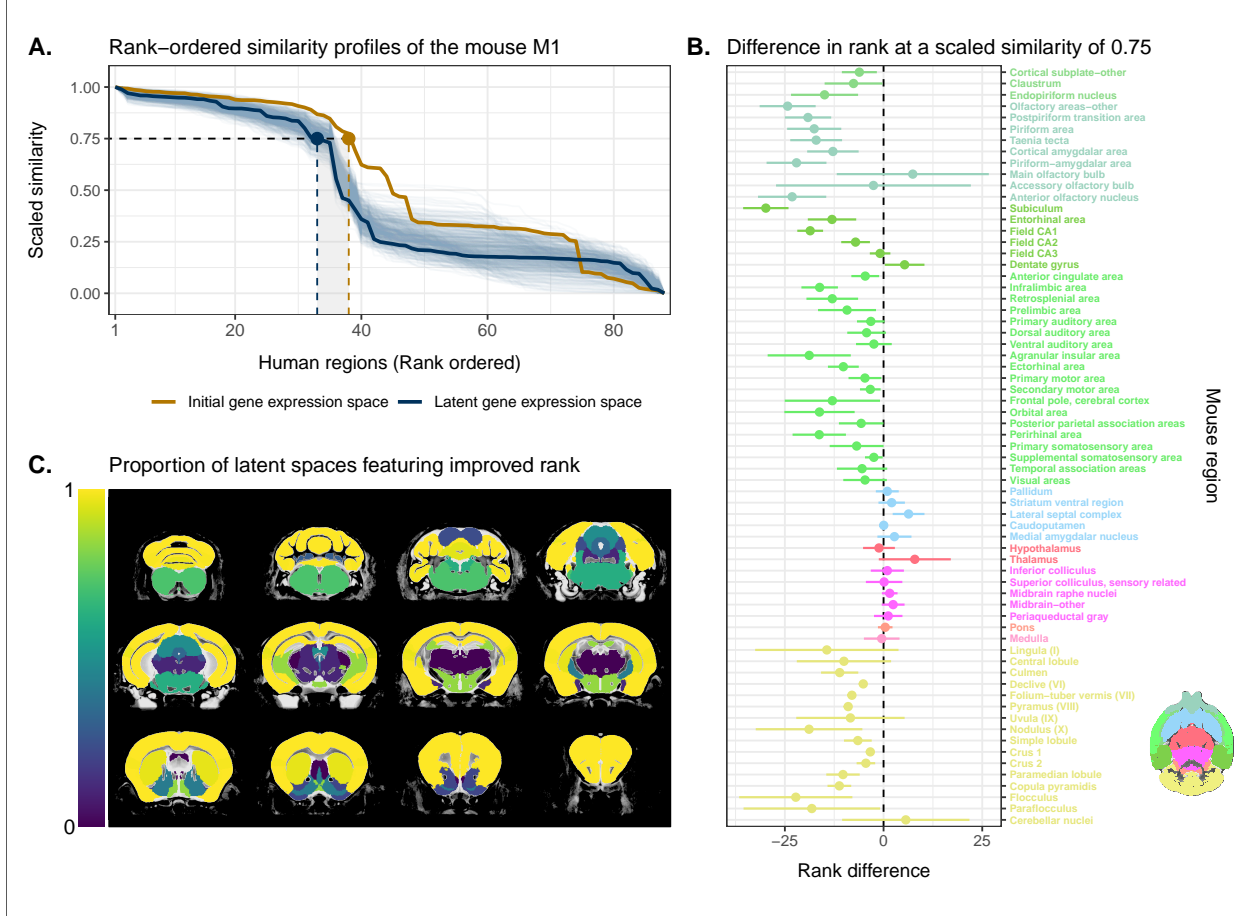


**Figure 3.** Quantifying improvement in locality in gene expression latent space. **(A)** The amount of local signal within a broadly similar region of the brain for a finer seed region's (e.g. primary motor area) similarity profile can be quantified by the decay rate of the head of the rank-ordered profile. Decay rate was quantified by computing the rank at a similarity of 0.75. This metric was compared between the initial gene expression space (orange line) and every gene expression latent space resulting from repeated training of the neural network (every blue line is a training outcome, heavy blue line serves as an example). A negative difference between these rank metrics indicates an improvement in locality in the latent space. **(B)** Structure-wise distributions of differences in rank at a similarity of 0.75 between the initial gene expression space and the gene expression latent spaces. Points and error bars represent mean and 95% confidence interval. Dashed black line at 0 indicates the threshold for improvement in one space over the other. Colours correspond to AMBA annotations as in Figures 1 and 2. Binomial likelihood (logistic regression) estimate of  $p = 0.78$  with %95 CI [0.66, 0.86]. **(C)** Proportion of perceptron training runs resulting in an improvement or null difference in the gene expression latent space compared with the initial space, estimated using region-wise logistic regressions. Cortical and cerebellar regions exhibit high proportions of improvement, while subcortical regions are less likely to be improved by the classification process.

262 probability of  $p = 0.5$ . We also evaluated the model for each brain region and found that 21 of the 36 regions  
263 (58%) return probability estimates of at least  $p = 0.80$  (Figure 4B). We find pronounced improvement in  
264 regions such as the piriform area, the subiculum, the primary motor and somatosensory areas, and the crus  
265 2, all of which have an estimated probability of  $p = 1$  with no variance around this value. A number of  
266 regions also demonstrate improvement in a high proportion of latent spaces: the claustrum ( $p = 0.89$ , 95%  
267 CI [0.86, 0.92]), the primary auditory area ( $p = 0.88$ , 95% CI [0.84, 0.90]), the visual areas ( $p = 0.96$ , 95%  
268 CI [0.94, 0.98]), and the uvula ( $p = 0.92$ , 95% CI [0.89, 0.94]). Once again we find that many regions in  
269 the sub-cortex do not benefit greatly from the gene expression latent spaces, since the initial gene set was  
270 already recapitulating the appropriate match with maximal similarity. We find that the striatum ventral  
271 region, hypothalamus, thalamus and caudoputamen are maximally similar to their canonical matches in  
272 at least 90% of latent spaces. In such cases, the classification approach performs as well as the original  
273 approach. While these probability estimates provide a sense of how often an improvement is returned, it  
274 is important to note that many regions in this set exhibit a substantial degree of variance over the latent  
275 spaces in the ranking of the canonical pairs, e.g. the claustrum (mean rank of  $\mu = 13$ , 95% CI [1, 35]), the  
276 visual areas ( $\mu = 23$ , 95% CI [8, 37]), the paraflocculus ( $\mu = 17$ , 95% CI [1, 36]). This is especially apparent  
277 for cerebellar regions, indicating some instability in the neural network's ability to recover these matches.  
  
278 Together, these results demonstrate that the multi-layer perceptron classification approach improves our abil-  
279 ity to resolve finer scale mouse-human neuroanatomical matches within the broadly similar regions obtained  
280 using the initial gene expression space. By training a classifier to predict the atlas labels in one species, we  
281 were able to generate a new common space that amplified the amount of local signal within broadly similar  
282 regions while also improving our ability to recover known mouse-human neuroanatomical pairs.

### 283 **Cortical areas involved in sensorimotor processing show greater transcriptomic 284 similarity than supramodal areas**

285 It is well established that the brains of most, if not all, extant mammalian species follow a common organi-  
286 zational blueprint inherited from an early mammalian ancestor (Kaas, 2011a). A number of cortical subdivi-  
287 sions have consistently been identified in members of many distantly related mammalian species (Krubitzer,  
288 2007) and hypothesized to have been present in the common ancestor of all mammals (Kaas, 2011a). While  
289 it is clear that basic sensorimotor cortical regions are found in the majority of mammals, including mice and  
290 humans, there is much debate about the extent to which cortical areas involved in supramodal processing  
291 are conserved across mammalian taxa. Although some supramodal regions were likely present in the earliest

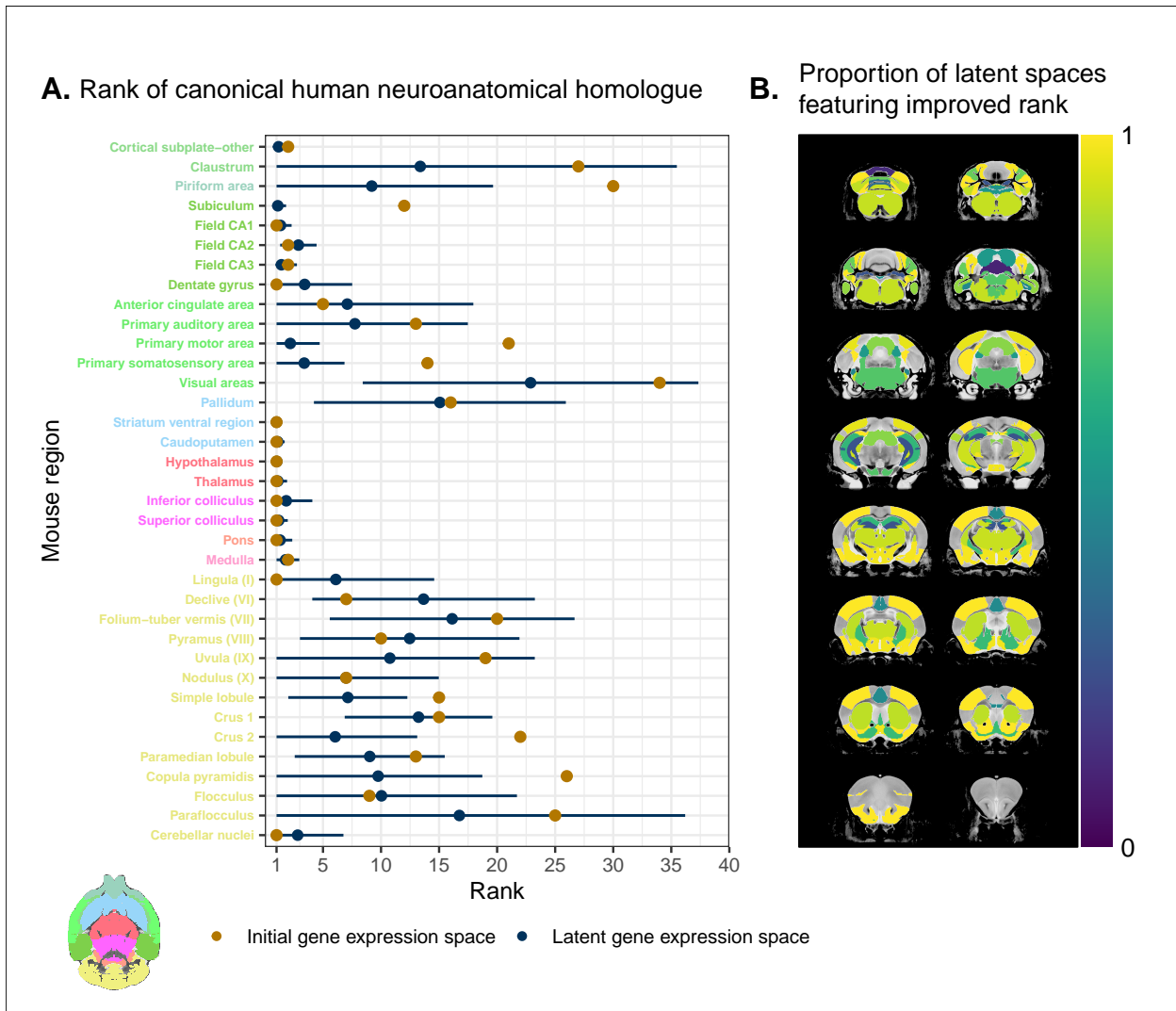


**Figure 4.** Recovering canonical neuroanatomical pairs in gene expression space. **(A)** Comparison between the ranks of canonical human matches for mouse seed regions between the initial gene expression space and gene expression latent spaces. Points and error bars represent mean and 95% confidence interval. Intervals are truncated at a minimal rank of 1, since values below this are meaningless. Mouse region names are coloured according to the AMBA palette. Binomial likelihood estimate of  $p = 0.58$  with 95% CI [0.42, 0.73]. **(B)** Proportion of latent spaces resulting in an improvement or null difference compared with the initial gene space, estimated using region-wise logistic regressions. Uncoloured voxels correspond to regions with no established canonical human match.

292 mammals, including some cingulate regions and an orbitofrontal cortex (Kaas, 2011a), since the divergence  
293 of mouse and human lineages some 80 million years ago, the primate neocortex has undergone substantial  
294 expansion and re-organization (Kaas, 2012). Indeed, when comparing the human neocortex even to primate  
295 model species, this is the likely locus of areas that cannot be easily translated between species (Rogier B.  
296 Mars et al., 2018b). As a result, it is important to investigate whether our between-species mapping is more  
297 successful in somatosensory areas than supramodal areas.

298 We assessed the similarity between mouse and human isocortical areas using the pairwise correlations in each  
299 of the gene expression latent spaces returned from the multi-layer perceptron. For every region in the mouse  
300 isocortex, we evaluated the distribution of maximal correlation values over latent spaces (Figure 5A). While  
301 the region-wise variance for each isocortical area was large, we found that, on average, sensorimotor regions  
302 exhibited higher maximal correlation values than supramodal regions (linear regression with binary predictor:  
303  $t(17) = -2.009, p = 0.0606$ ). The mouse primary somatosensory ( $r = 0.97$  with 95% CI [0.94, 0.99]) and  
304 motor areas ( $r = 0.94$  with 95% CI [0.89, 0.98]) have the highest average maximal correlation values. We  
305 additionally examined the distributions of maximal correlation, grouped by cortex type (Figure 5B). To  
306 generate these distributions, we computed average maximal correlation values by cortex type in each of the  
307 latent spaces. Here too we find that sensorimotor regions are associated with higher maximal correlation  
308 values on average compared with supramodal areas (linear mixed-effects regression:  $t(499) = -46.8, p <$   
309  $2 \cdot 10^{-16}$ ). These distributions demonstrate that sensorimotor isocortical regions exhibit more similarity  
310 overall on the basis of homologous gene expression than do supramodal regions.

311 While we found that sensorimotor isocortical areas in the mouse brain were more similar to human brain  
312 regions than supramodal areas, the distributions of maximal correlation do not speak to the neuroanatomical  
313 patterns of organization for these matches. To understand how the similarity patterns of mouse and human  
314 cortical subdivisions were organized, we used hierarchical clustering to cluster mouse and human isocortical  
315 regions on the basis of their similarity profiles in the average gene expression latent space (Figure 5C). This  
316 allows us to examine the similarity of regions to one another within and across brains at multiple levels  
317 simultaneously.

318 At a high level, we find a striking segregation of the mouse isocortex into one main cluster that corresponds  
319 to regions that are primarily engaged in sensorimotor processing and separate clusters of regions that are  
320 supramodal. All of the sensorimotor areas cluster together, but two supramodal areas also form part of this  
321 cluster: the posterior parietal association areas and the anterior cingulate cortex. The mouse sensorimotor  
322 cluster is characterized by high correlation values to human sensorimotor regions like the precentral gyrus, the  
323 cuneus, and the postcentral gyrus, as well as low correlation values to the piriform cortex and paraterminal

324 gyrus. At this level of clustering, the remaining mouse supramodal subdivisions form three clusters, though  
325 two of these each only contain one region. The retrosplenial and infralimbic areas each belong to their own  
326 unique clusters. The similarity profile of the retrosplenial area is most similar to the sensorimotor cluster,  
327 and these two clusters are combined in the three-cluster solution. The remaining two mouse clusters are  
328 characterized by low correlations to the human cluster containing sensorimotor areas. The infralimbic area  
329 additionally exhibits low correlation to the majority of human regions.

330 On the human side, the four-cluster solution also features a sensorimotor cluster, which contains regions  
331 like the pre- and post-central gyri, the cuneus, and Heschl's gyrus. This cluster exhibits a high degree  
332 of similarity to the mouse sensorimotor cluster and low similarity to the mouse supramodal clusters. The  
333 cortical regions not belonging to this cluster are split into three clusters. The majority of these remaining  
334 regions cluster together in a large cluster that contains regions like the cingulate gyrus and the frontal pole.  
335 The parolfactory gyri, parahippocampal gyrus and temporal pole form a separate cluster that exhibits high  
336 correlation to the mouse ectorhinal area, while the paraterminal gyrus and piriform cortex are clustered  
337 together and highly similar to the mouse infralimbic area.

338 We additionally ran hierarchical clustering on the isocortical similarity matrix in the original homologous  
339 gene space. While the cluster annotations were not substantially different in this space, we observed that  
340 the Euclidean distances within and between clusters were smaller compared with the latent space clustering,  
341 further confirming that the perceptron classification approach improves the segregation of brain regions in  
342 the gene expression common space (Figure 5D).

343 Overall, we observe a greater degree of similarity between mouse and human cortical regions involved in  
344 basic sensorimotor processing compared with supramodal or association areas. This is in line with the large  
345 body of existing research that suggests that sensory and motor areas of the cortex are conserved across the  
346 brains of mammals. While sensorimotor areas exhibit a greater degree of similarity than supramodal areas,  
347 the neuroanatomical pattern of correspondences obtained using mouse-human homologous genes is not at  
348 the level of individual cortical areas. Still, using a clustering approach we identified clear distinctions in  
349 the patterns of similarity between sensorimotor and supramodal areas, especially for regions in the mouse  
350 isocortex.

### 351 **Transcriptomic comparison of the mouse and human striatum**

352 We have focused here on comparing mouse and human brain organization using transcriptomic data, with  
353 a latent space based on homologous genes as the common space between the two species. To date, common

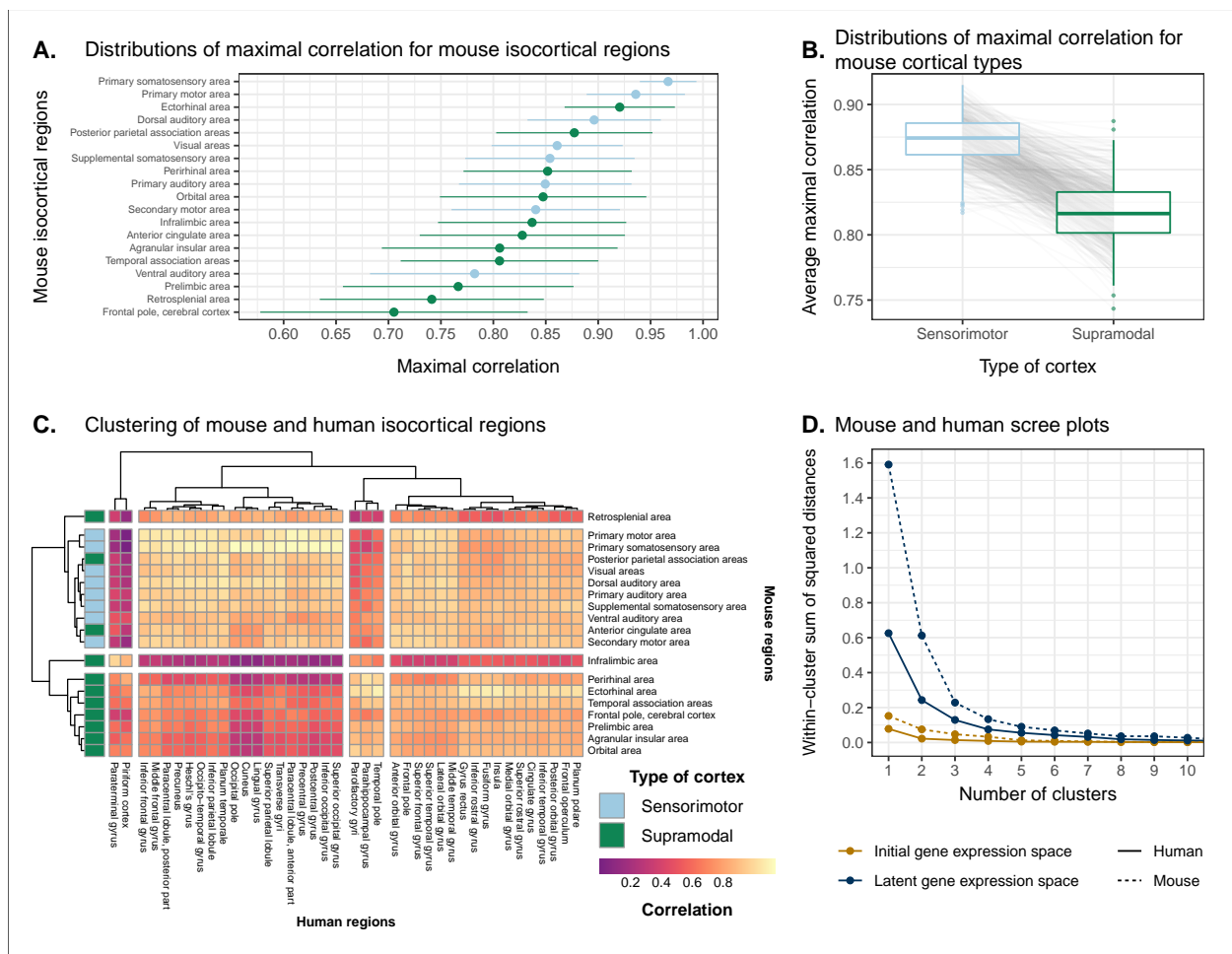


**Figure 5.** Similarity of mouse-human isocortical regions. (A) Maximal correlation distributions of mouse isocortical regions. Points and error bars represent mean and 95% confidence interval over latent space samples. Linear regression using average maximal correlation values:  $t(17) = -2.009$ ,  $p = 0.0606$ . (B) Distributions of average maximal correlation for sensorimotor and supramodal isocortical areas in each gene expression latent space. Grey lines correspond to individual latent spaces. Linear mixed-effects regression:  $t(499) = -46.8$ ,  $p < 2 \cdot 10^{-16}$ . (C) Hierarchical clustering of mouse and human isocortical regions based on average latent space correlation values. Mouse regions are annotated as sensorimotor or supramodal. Four clusters were chosen for visualization using the elbow method. (D) Within-cluster sum of squared distances for different numbers of mouse and human isocortical clusters in the average latent space and initial homologous gene space.

space comparisons between the mouse and human brain have only been performed using functional connectivity (Balsters et al., 2020; Schaeffer et al., 2020). As a case in point, Balsters et al. (2020) compared mouse and human striatal organization using this measure. They found that the nucleus accumbens was highly conserved between mice and humans, and that voxels in the posterior part of the human putamen were significantly similar to the lateral portion of their mouse caudoputamen parcellation. Additionally, they report that 85% of voxels in the human striatum were not significantly similar to any of their mouse striatal seeds, and that 25% of human striatal voxels were significantly dissimilar compared with the mouse. These differences were understandable, as they involved parts of the human striatum that connected to parts of prefrontal cortex that have no known homolog in the mouse (Neubert et al., 2014). However, it is not necessarily the case that between-species differences in connectivity are associated with distinct architectonic or molecular signatures. Therefore, we investigated the patterns of similarity between the mouse and human striata on the basis of gene expression using the neural network latent space representations.

We first identified the striatal regions present in the Allen human dataset: the caudate, the putamen, and the nucleus accumbens. We evaluated the correlation between the microarray samples in these regions and every region in the mouse atlas. Based on these correlation values, we focused our analysis on the four mouse regions that were consistently the most similar across all latent spaces: the caudoputamen, the nucleus accumbens, the fundus of striatum, and the olfactory tubercle. For each of the human striatal regions, we then calculated the average correlation over the samples to each of the mouse targets. We examined the distribution of these average correlation values over the latent spaces (Figure 6A). We find that the human caudate and putamen consistently exhibit the strongest degree of similarity to the mouse caudoputamen. The median of the distribution for the caudate-caudoputamen pairs is 0.95 and 0.97 for the putamen-caudoputamen pairs, with modal values of 0.94 and 0.97, respectively. All latent spaces return correlations greater than 0.9 for caudate-caudoputamen and putamen-caudoputamen pairs. Beyond this expected top match, the caudate and putamen both exhibit high similarity to the nucleus accumbens and the fundus of striatum, with mean correlation values of about 0.80. Neither of these target regions is consistently more similar to the mouse caudoputamen over all latent spaces.

While the similarity of the caudate and the putamen to the caudoputamen is unsurprising, the story is not as clear for the human nucleus accumbens. We find that the variance in correlation calculated over all mouse targets is much lower ( $\sigma = 0.04$ ) compared with the equivalent variances for the caudate ( $\sigma = 0.09$ ) and putamen ( $\sigma = 0.10$ ), indicating less specificity to any one mouse striatal target. In particular, the human nucleus accumbens isn't as specifically similar to the mouse nucleus accumbens in the way that the caudate and putamen are similar to the caudoputamen. The mouse target distributions are right-shifted compared

386 with those for the caudate and putamen, with mean values of 0.90, 0.89, and 0.89 for the mouse nucleus  
387 accumbens, caudoputamen, and fundus of striatum, respectively. The human accumbens also exhibits a high  
388 degree of similarity to the mouse olfactory tubercle, the distribution of which is also right-shifted compared  
389 with the caudate and putamen.

390 Given the high correlation of the human caudate and putamen to the mouse caudoputamen, as well as the  
391 finding reported by Balsters et al. about the similarity of the lateral caudoputamen to the putamen, we were  
392 curious as to whether we could identify sub-regional patterns of similarity in the caudoputamen and other  
393 striatal regions using these gene expression data. To probe this question, we first examined the average latent  
394 space correlation between each voxel in the mouse striatum and every region in the human atlas. We created  
395 brain maps for the human regions that exhibited the highest mean correlation values, averaged over mouse  
396 striatal voxels: the caudate, the putamen, the nucleus accumbens, and the septal nuclei (Figure 6B). We find  
397 that voxels in the caudoputamen exhibit a homogeneous pattern of similarity to both the caudate and the  
398 putamen. On average, voxels in the caudoputamen have a correlation of 0.95 to the caudate and 0.94 to the  
399 putamen, with standard deviations of 0.04 and 0.05 respectively. The caudate and putamen are associated  
400 with correlations of at least 0.90 in 88% and 84% of caudoputamen voxels. A number of voxels are also  
401 highly similar to the human nucleus accumbens, with an average correlation value of 0.90 and 55% of voxels  
402 returning a correlation of at least 0.9. The caudoputamen voxels most similar to the nucleus accumbens lie  
403 in the ventral-rostral part of the region. Of course, voxels in the mouse nucleus accumbens are also highly  
404 similar to the human nucleus accumbens, with an average of 0.90 and standard deviation of 0.06. While the  
405 human nucleus accumbens is the most strongly correlated region, a number of voxels also exhibit reasonably  
406 strong correlations to the substantia innominata, the septal nuclei, and the amygdala. Indeed, 91% of voxels  
407 in the accumbens are correlated at a value of 0.7 or higher to the substantia innominata. The equivalent  
408 percentages for the septal nuclei and amygdala are 78% and 74% respectively.

409 We additionally examined the proportion of latent spaces in which each voxel in the mouse striatum was  
410 maximally similar to the human target regions (Figure 6C). As expected, we find that voxels in the cau-  
411 doputamen are most often maximally similar to the human caudate and putamen, with 75% of voxels in  
412 the caudoputamen being maximally similar to the caudate or putamen in at least 95% of latent spaces, and  
413 62% of voxels being maximally similar to one of those targets in all latent spaces. Interestingly, we observe  
414 the emergence of a continuous bilateral pattern of specificity to the caudate and putamen, with voxels in  
415 the rostral and lateral-caudal parts of the caudoputamen being more specific to the caudate, and voxels in  
416 the medial-rostral part being more specific to the putamen. This map highlights subtle differences in the  
417 similarity between caudoputamen voxels and the caudate or putamen. While this pattern distinguishes the

418 two regions on the basis of which is the top match, individual voxels have very similar correlation values to  
419 the targets (Figure 6B), with a mean difference in correlation of only 0.006. Beyond the caudoputamen, we  
420 find that the accumbens and olfactory tubercle in the mouse are consistently similar to the human nucleus  
421 accumbens, with 80% of mouse accumbens voxels and 65% of olfactory tubercle voxels having the human  
422 accumbens as their top match in at least 80% of latent spaces. For those voxels below this threshold, the  
423 human regions that are most often the top match are once again the amygdala, the septal nuclei, and the  
424 substantia innominata.

425 Overall, we observe a strong association between the mouse caudoputamen and both the human caudate and  
426 putamen. While we find a subtle pattern of specificity to either region among voxels in the caudoputamen on  
427 the basis of maximal similarity, the high degree of similarity in the correlation values to each region suggests  
428 that the majority of voxels in the caudoputamen are equally similar to the caudate and the putamen on the  
429 basis of the expression of mouse-human homologous genes. We also find that the nucleus accumbens is well  
430 conserved across species. However the region also exhibits patterns of similarity that go beyond the simple  
431 one-to-one match. The human accumbens features similar correlation values to the mouse caudoputamen  
432 and fundus of striatum, in addition to the accumbens proper, with no sharp distinction between these regions.  
433 It also exhibits a larger degree of similarity to the mouse olfactory tubercle. This is also seen in the mouse  
434 striatum, where voxels in the accumbens and the olfactory tubercle map onto the human accumbens.

## 435 Discussion

436 We have demonstrated how spatial transcriptomic patterns of homologous genes can be used to make quan-  
437 titative comparisons between the mouse and human brain. We showed that using homologous genes as a  
438 common space allows one to easily identify coarse similarities in brain structures across species, but that  
439 more fine-scaled parcellations, such as at the level of cortical areas, are more complex. Despite this limi-  
440 tation, the approach still allows for a formal assessment of different patterns of between-species similarity  
441 in primary compared to supramodal regions, identifications of distinct clusters of cortical territories across  
442 species, and comparison of between-species similarities at the transcriptomic level to those observed using  
443 other modalities. We will discuss our observations in the context of the importance of the mouse as a model  
444 for human neuroscience below.

445 The abundance of neuroscience research performed using mice has resulted in a wealth of knowledge about the  
446 mouse brain. In the preclinical setting, mouse models are utilized with the intention of better understanding  
447 human neuropathology. For instance, in the context of autism spectrum disorders, a plethora of studies

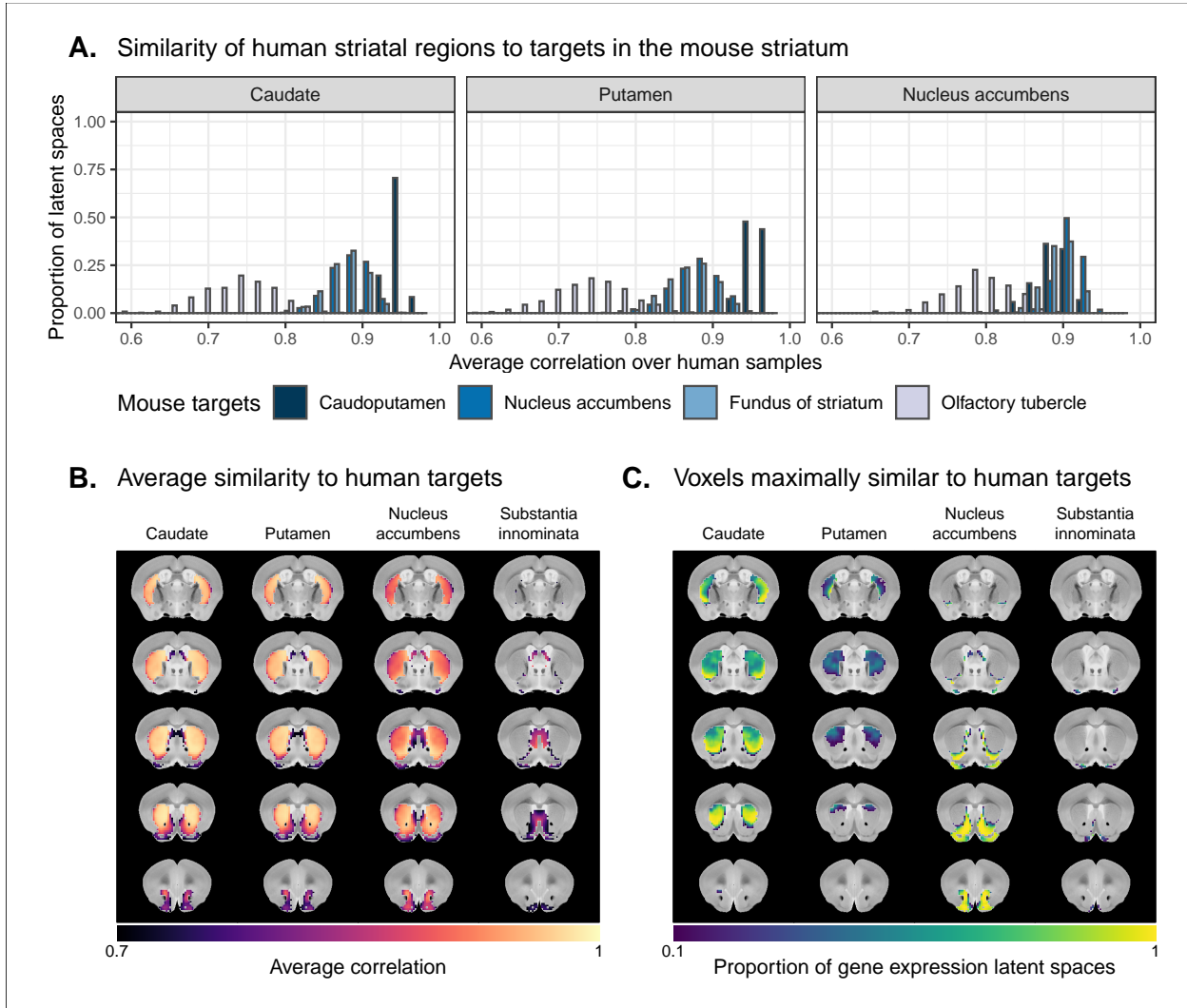


**Figure 6.** Similarity among mouse and human striatal regions. **(A)** Distributions over gene expression latent spaces of region-wise average correlation values for mouse and human striatal pairs. Human regions were chosen based on the AHBA ontology. Mouse target regions were chosen to be those with the highest average correlation values. **(B)** Latent space averaged correlations between voxels in the mouse striatum and human target regions. Target regions were selected based on the highest mean correlation across all striatal voxels. **(C)** Proportions of latent spaces in which mouse striatal voxels are maximally similar to human target regions.

448 using mouse models have reported on the neurobiological and neuroanatomical phenotypes that arise from  
449 mutations at specific genetic loci (Gompers et al., 2017; Horev et al., 2011; Pagani et al., 2021). It is common  
450 for researchers involved in translational neuroscience to rely on findings of this kind to make inferences about  
451 the human disorder. The typical approach, which is to identify rough post-hoc correspondences between  
452 neuroanatomical ontologies, is not particularly comprehensive and is subject to confirmation bias. While it  
453 may be a reasonable starting point for comparison, the true correspondence between the mouse and human  
454 brain is likely more complicated given the evolutionary distance between the two species. Although overall  
455 patterns of brain organization, including the general pattern of neocortical organization, are similar across  
456 all mammals, substantial differences are evident (Ventura-Antunes et al., 2013). To make matters worse,  
457 researchers from the different neuroscientific traditions often use distinct terminology, further complicating  
458 detailed information exchange. To address these problems, we sought to establish a first quantitative whole-  
459 brain comparison between the two species.

460 The expression of homologous genes provides an elegant way to define a common space for quantitative cross-  
461 species comparisons since it relies on homology at a deep molecular biological level. The approach is not  
462 without limitations however. First, the acquisition of whole-brain transcriptomic data is labour-intensive,  
463 time consuming, and invasive. These data sets cannot be generated easily, especially in the human, in which  
464 the process depends on the availability of post-mortem samples. As a result, the effective sample sizes are  
465 extremely limited in this domain. For instance, in the Allen mouse coronal in-situ hybridization data set  
466 used here, the brain-wide expression of each gene is sampled only once (barring a few exceptions). This  
467 constrains the types of analyses that are possible (e.g. null hypothesis significance testing) and largely limits  
468 the availability of replication data sets. That being said, new technologies, such as spatial transcriptomics,  
469 are gradually making it easier to acquire brain-wide gene expression data in less time and at lower cost (Ortiz  
470 et al., 2020; Stahl et al., 2016; Vickovic et al., 2019). Second, the approach of relying on all available genes  
471 is subject to noise. To address this issue, Myers (2017) (Myers, 2017) used a method of gene set selection  
472 to attempt to improve the correspondence between established mouse-human homologies. While this lead  
473 to improvement, it was only at the level of coarsely defined regions (e.g. cortex-cortex). Our approach,  
474 therefore, was to use supervised machine learning to create a latent common space based on combinations  
475 of homologous genes that can delineate areas within a single species.

476 This latent common space approach led to a substantial improvement in specificity of between-species com-  
477 parisons. Nevertheless, it is evident that the first major distinction in gene expression patterns within a  
478 species, and the easiest identification of similarity across species, is at the coarse anatomical level of the  
479 major subdivisions of the vertebrate brain, such as the isocortex, cerebellar hemispheres and nuclei, and

480 brain stem. All of these territories were present in the ancestral vertebrate brain (Striedter and Northcutt,  
481 2020) and the ability to detect conserved transcriptomic signatures at this level is not surprising. Within  
482 such structures, such as the isocortex, our ability to make simple one-to-one correspondences decreased. This  
483 is partly because areas within a coarse structure have more similar transcriptomic profiles, but also likely  
484 due to the fact that a single area in one brain does not have a single correspondent in another, larger brain.  
485 In other words, regions in the brains of related species may exhibit one-to-many or many-to-many mappings.  
486 In our study, we found greater cross-species similarity between cortical areas associated with sensorimotor  
487 processing than areas in supramodal cortex. Primary areas, including the sensorimotor areas, are present  
488 in all mammals studied to date and likely part of the common ancestors of all mammals (Kaas, 2011a;  
489 Krubitzer, 2007). Although this common ancestor likely also had non-primary areas, it cannot be denied  
490 that association cortex expanded dramatically in primates and especially so in the human brain (Chaplin et  
491 al., 2013; Mars et al., 2016a). Again, the pattern found here of greater similarity in more conserved areas  
492 might reflect this evolutionary history. In that context it is interesting to note that some non-primary areas  
493 thought to be present in the common mammalian ancestor, such as cingulate and orbitofrontal cortex (Kaas,  
494 2011a) showed relatively high correlation to human areas.

495 An advantage of the approach presented here is that it can, in principle, be applied to any aspect of brain  
496 organization. Beyond simply establishing whether areas are similar across species in a particular common  
497 space, comparing the results across common spaces established using different types of neuronal data can  
498 inform on which larger principles of organization are similar across brains (Eichert et al., 2020). This is  
499 illustrated here by the results of our striatal analysis. We found high similarity between the human caudate  
500 and putamen and mouse caudoputamen, with little differentiation within these regions in a single species.  
501 In contrast, Balsters et al. (2020) demonstrated that human caudoputamen contains a distinct pattern of  
502 connectivity. At first sight, one could argue the results are in contrast. However, evolutionarily speaking, it  
503 is quite probable that an overall similar transcriptomic signature of the striatum can be accompanied by a  
504 distinct connectivity pattern to areas of the cortex present in only one of the two species. Indeed, this speaks  
505 to the different types of similarity that can be studied, depending on which aspect of brain organization one  
506 is interested in. Although the human brain is much larger than the mouse brain and contains a number  
507 of cortical territories that have no homologue in the mouse brain (Kaas, 2011b; Rudebeck and Izquierdo,  
508 2022), the similarity in transcriptomic signature mean that translations between the species is valid in many  
509 contexts.

510 The power of a formal understanding of similarities and differences between brains at different levels of  
511 organization is evident. In fundamental neuroscience, it will help translate results from data types that

512 cannot be obtained in humans to the human brain (Barron et al., 2021). In translational neuroscience, it  
513 will, in a negative sense, help establish the limits of the translational paradigm by showing which aspects  
514 of the human brain cannot be understood using the model species (Liu et al., 2021). In a positive sense,  
515 it will also help by establishing and improving our understanding of the many aspects in which the model  
516 and human brain do concur (Mandino et al., 2021). More ambitious still, it can provide a way in which  
517 highly diverse manifestations of certain disease syndromes (e.g. autism spectrum disorder) (Grzadzinski et  
518 al., 2013; Simonoff et al., 2008) and the availability of many distinct model strains (Ellegood et al., 2015),  
519 each hypothesized to capture a distinct aspect of a multi-dimensional clinical syndrome, can be related to  
520 one another. Ultimately, we believe that using the mapping of homologous gene expression between species  
521 can be an important part of building a transform that maps information obtained using mice to humans and  
522 vice versa.

## 523 Materials and methods

### 524 Mouse gene expression data

525 We used the adult mouse whole-brain in-situ hybridization data sets from the Allen Mouse Brain Atlas  
526 (Lein et al., 2007). Specifically, we used 3D expression grid data, i.e. expression data aligned to the Allen  
527 Mouse Brain Common Coordinate Framework (CCFv3)(Wang et al., 2020) and summarized under a grid  
528 at a resolution of  $200\mu m$ . We downloaded the gene expression “energy” volumes from both the coronal  
529 and sagittal in-situ hybridization experiments as a sequence of 32-bit float values using the Allen Institute’s  
530 API (<http://help.brain-map.org/display/api/Downloading+3-D+Expression+Grid+Data>). These volumes  
531 were subsequently reshaped into 3D images in the MINC format. Origin, extents, and spacing were defined  
532 such that the image was RAS-oriented, with the origin at the point where the anterior commissure crosses  
533 the midline. The MINC images from the coronal and sagittal data sets were then processed separately  
534 using the Python programming language. The sagittal data set was first filtered to keep only those genes  
535 that were also present in the coronal set. Images were imported using the `pyminc` package, masked and  
536 reshaped to form an experiment-by-voxel expression matrix. We pre-processed this data by first applying a  
537 `log2` transformation for consistency with the human data set. For those genes associated with more than  
538 one in-situ hybridization experiment, we averaged the expression of each voxel across the experiments. We  
539 subsequently filtered out genes for which more than 20% of voxels contained missing values. Finally, we  
540 applied a K-nearest neighbours algorithm to impute the remaining missing values. The result of this pre-  
541 processing pipeline was a gene-by-voxel expression matrix with 3958 genes and 61315 voxels for the coronal

542 data set and a matrix with 3619 genes and 26317 voxels for the sagittal data set.

## 543 Human gene expression data

544 Human gene expression data was obtained from the Allen Human Brain Atlas (Hawrylycz et al., 2012).  
545 The data were downloaded from the Allen Institute’s API (<http://api.brain-map.org>) and pre-processed  
546 using the `abagen` package in Python (<https://abagen.readthedocs.io/en/stable/>) (Arnatkeviciūtė et al., 2019;  
547 Hawrylycz et al., 2012; Markello et al., 2021). We used the microarray data from the brains of all six donors,  
548 each of which contains `log2` expression values for 58692 gene probes across numerous tissue samples. The  
549 pre-processing pipeline included probe selection using differential stability on data from all donors and  
550 intensity-based filtering of probes at a threshold of 0.5. The samples and genes were additionally normalized  
551 for each donor individually using a scaled robust sigmoid function. In practice, this pipeline was implemented  
552 using the `get_samples_in_mask` function from the `abagen` package. The remaining parameters were set to  
553 their default values. The output of the pre-processing pipeline was a gene-by-sample expression matrix with  
554 15627 genes and 3702 samples across all donors.

## 555 Mouse atlases

556 We used a version of the DSURQE atlas from the Mouse Imaging Centre (Dorr et al., 2008; Qiu et al., 2018;  
557 Richards et al., 2011; Steadman et al., 2014; Ullmann et al., 2013), modified using the AMBA hierarchical  
558 ontology, which was downloaded from the Allen Institute’s API. The labels of the DSURQE atlas correspond  
559 to the leaf node regions in the AMBA ontology, which allowed us to use the hierarchical neuroanatomical  
560 tree to aggregate and prune the atlas labels to the desired level of granularity. For the purposes of our  
561 analyses, we removed white matter and ventricular regions entirely. The remaining grey matter regions were  
562 aggregated up the hierarchy so that the majority of resulting labels contained enough voxels to be classified  
563 appropriately by the multi-layer perceptron. In doing so, we maintained approximately the same level of  
564 tree depth within a broad region (e.g. cerebellar regions were chosen at the same level of granularity). This  
565 resulted in a mouse atlas with 67 grey matter regions. We additionally generated an atlas with 11 broader  
566 regions for visualization and annotation purposes.

## 567 Human atlases

568 We used the hierarchical ontology from the AHBA, which we obtained using the Allen Institute’s API.  
569 We aggregated and pruned the neuroanatomical hierarchy to correspond roughly to the level of granularity

570 obtained in our mouse atlas, resulting in 88 human brain regions. We additionally generated a set of 16  
571 broad regions for visualization and annotation. White matter and ventricular regions were omitted entirely.

## 572 **Regional expression and similarity matrices**

573 We created the mouse and human gene-by-region expression matrices from the mouse gene-by-voxel and  
574 human gene-by-sample expression matrices. First, we intersected the gene sets in these matrices with a  
575 list of 3331 homologous genes obtained from the NCBI HomoloGene database (NCBI, 2018), resulting in  
576 2835 homologous genes present in both the mouse and human expression matrices. We then annotated  
577 each of the human samples with one of the 88 human atlas regions, and each of the mouse voxels with  
578 one of the 67 mouse atlas regions, discarding white matter and ventricular entries in the process. These  
579 labelled expression matrices were subsequently normalized as follows: For each matrix, we first standardized  
580 every gene across all voxels/samples using a z-scoring procedure. We then centered every voxel/sample  
581 by subtracting the average expression over all homologous genes. Finally, we generated the gene-by-region  
582 expression matrices by averaging the expression of every gene over the voxels/samples corresponding to  
583 each atlas region. Using these expression matrices, we generated the mouse-human similarity matrix by  
584 computing the Pearson correlation coefficient between all pairs of mouse and human regions.

## 585 **Gene enrichment analysis**

586 We ran a gene enrichment analysis on the set of homologous genes obtained from the NCBI HomoloGene  
587 database. We first downloaded Gene Ontology data for biological process related modules from the Bader  
588 Lab at the University of Toronto (<http://baderlab.org/GeneSets>). These data include a gene set of 16563  
589 genes and a module set of 15757 biological process modules. Every module is associated with a subset  
590 of genes from the full gene set. For each module, we used a hypergeometric test to evaluate whether the  
591 homologous gene set was over-represented in the module subset, compared with the full gene set. The  
592 resulting p-values were adjusted for multiple comparisons using the false-discovery rate method (Benjamini  
593 and Hochberg, 1995). A total of 938 modules were found to be significant at a threshold of 0.001. The  
594 surviving modules were ordered according to their p-values and written out to a comma-separated values  
595 data file (Supplementary File 1). This analysis was carried out using the `tmod` package in the R programming  
596 language.

597 **Multi-layer perceptron classification and latent space**

598 To improve the resolution of mouse-human neuroanatomical matches, we performed a supervised learning  
599 approach, wherein we trained a multi-layer perceptron neural network to classify 67 mouse atlas regions  
600 from the expression values of 2835 homologous genes. We chose a model architecture in which each layer  
601 of the network was fully connected to previous and subsequent layers. To optimize the hyperparameters,  
602 we implemented an ad hoc cross-validation procedure that took into account the fact that the majority of  
603 genes in the coronal AMBA data set are sampled only once over the entire mouse brain. The procedure  
604 involved a combination of the coronal data set and the sagittal in-situ hybridization data sets. For the  
605 sagittal data set, we used the expression matrix described above. However, we used a modified version  
606 of the coronal expression matrix. This matrix was generated using the pipeline described above with the  
607 following modifications: 1. We applied a *unilateral* brain mask to the coronal images since the sagittal data  
608 is unilateral by construction, and 2. we did not aggregate the expression of multiple in-situ hybridization  
609 experiments for those genes in the coronal set pertaining to more than one experiment. We then filtered  
610 these experiment-by-voxel expression matrices according to the list of mouse-human homologous genes, as  
611 well as the human sample expression matrix. We also annotated the voxels in each of the expression matrices  
612 with one of the 67 regions in the mouse atlas. Our validation procedure then involved iterative construction  
613 of training and validation sets by sampling gene experiments from either the coronal or sagittal matrices: For  
614 every gene in the homologous set, we first determined whether that gene was associated with more than one  
615 experiment in the coronal matrix. If this was the case, we randomly sampled one of those experiments for the  
616 training set and one of the remaining experiments for the validation set. If the gene was associated with only  
617 one experiment in the coronal set, we randomly sampled either the coronal or sagittal experiment for the  
618 training set and the other for the validation set. Once the training and validation sets were generated, they  
619 were normalized using the procedure described above. We then trained the neural network using the training  
620 set and evaluated its performance on the validation set. Given that the construction of the training and  
621 validation sets involved some stochasticity, we repeated this construction, training, and validation procedure  
622 10 times for every combination of hyperparameters.

623 The hyperparameters that we optimized using this method were the number of hidden layers in the network,  
624 the number of hidden units (i.e. neurons) per hidden layer, the dropout rate, and the amount weight decay.  
625 The values we optimized over were as follows. We varied the number of hidden layers between 3 and 5. We  
626 varied the number of hidden units between 100 and 1000 in increments of 100. For the dropout rate, we  
627 examined values of 0, 0.25 and 0.50. For the amount of weight decay, we examined values of  $10^{-6}$  and  $10^{-5}$ .  
628 We found that the best-performing model had 3 hidden layers, 200 neurons per layer, a dropout rate of 0,

629 and a weight decay value of  $10^{-6}$ . This model returned an average classification accuracy of 0.926 on the  
630 training sets and of 0.526 on the validation sets. Following validation, we used the optimal hyperparameters  
631 to train the network on the full bilateral coronal voxel-wise expression matrix.

632 These models were implemented in Python using PyTorch via the `skorch` library (<https://skorch.readthedocs.io/en/stable/>). For both validation and training, the models were trained over 200 epochs  
633 using a maximum learning rate of  $10^{-5}$ . We used the `AdamW` optimization algorithm (Loshchilov and Hutter,  
634 2019) and `OneCycleLR` learning rate scheduler policy. The activation function used in the forward pass  
635 was the rectified linear unit (ReLU) and the loss function was the negative log-likelihood loss, which is the  
636 default for the `NeuralNetClassifier` class in `skorch`.

638 We used the trained perceptron to generate the latent gene expression space. To extract the appropriate  
639 transformation, we removed the predictive output layer and soft-max transformation from the network  
640 architecture. The resulting architecture returns the 200 hidden units in the third hidden layer as the output  
641 of the network. To create the latent space data representations, we applied this network to the mouse  
642 and human gene-by-region expression matrices, transposed so that the genes were the input variables. The  
643 resulting matrices have 200 columns corresponding to the hidden units and 67 (88) rows corresponding to  
644 the mouse (human) regions. They describe each brain region's weight over the hidden units. To create the  
645 similarity matrix, we calculated the Pearson correlation coefficient between all pairs of mouse and human  
646 regions.

647 Given the stochasticity inherent in training the network (e.g. random weight initialization and stochas-  
648 tic optimization), we repeated the training and transformation process 500 times using the same network  
649 architecture and input data.

## 650 Multi-layer perceptron feature importance

651 (WRITE THIS)

## 652 Quantifying improvement in gene expression latent spaces

653 To quantify the improvement in the locality and homology criteria for the common space, we used a logistic  
654 regression model to estimate the probability that the rank difference was less than or equal to zero. To  
655 estimate the overall improvement due to the latent spaces, we created a binary variable to encode whether  
656 the average rank difference over latent spaces for each region met the success criterion. This variable was

then used as our target in a logistic regression with no regressors. Once the model was fit, we applied the logistic function to the intercept parameter estimate to get the corresponding estimate for the Bernoulli probability  $p$ . This was also applied to the bounds on the variance estimate for the intercept to get the corresponding confidence interval. We additionally applied this approach on a region-wise basis to evaluate the likelihood of a region seeing improvement in the latent spaces. These models were implemented using the `glm` function from the `stats` package in the R programming language.

## 663 Data and code availability

664 This manuscript and all figures were generated programmatically using R Markdown (<https://rmarkdown.rstudio.com>) and L<sup>A</sup>T<sub>E</sub>X(<https://www.latex-project.org>). The Allen Mouse Brain Atlas and Allen Human  
665 Brain Atlas data sets are openly accessible and can be downloaded from the Allen Institute's API (<http://api.brain-map.org>). All of the code and additional data needed to generate this analysis, including figures  
666 and manuscript, is accessible at <https://github.com/abeaucha/MouseHumanTranscriptomicSimilarity/>.  
667

## 669 Acknowledgments

670 We thank C. Hammill, D.J. Fernandes, E. Anagnostou, B.J. Nieman, and E. Sibille for providing advice  
671 and for interesting conceptual discussions. This study was supported by the Canadian Institutes of Health  
672 Research (doctoral funding and foreign study award for A.B.). The Wellcome Centre for Integrative Neu-  
673 roimaging is supported by core funding from the Wellcome Trust (203139/Z/16/Z).

## 674 Competing interests

675 The authors declare that they have no competing interests.

## 676 References

- 677 Arnatkevičiūtė A, Fulcher BD, Fornito A. 2019. A practical guide to linking brain-wide gene expression and  
678 neuroimaging data. *NeuroImage* **189**:353–367. doi:10.1016/j.neuroimage.2019.01.011  
679 Balsters JH, Zerbi V, Sallet J, Wenderoth N, Mars RB. 2020. Primate homologs of mouse cortico-striatal  
680 circuits. *eLife* **9**:24. doi:10.7554/eLife.53680

- 681 Barron HC, Mars RB, Dupret D, Lerch JP, Sampaio-Baptista C. 2021. Cross-species neuroscience:  
682 Closing the explanatory gap. *Philosophical Transactions of the Royal Society B: Biological Sciences*  
683 **376**:20190633. doi:10.1098/rstb.2019.0633
- 684 Benjamini Y, Hochberg Y. 1995. Controlling the False Discovery Rate: A Practical and Powerful Approach  
685 to Multiple Testing. *Journal of the Royal Statistical Society Series B (Methodological)* **57**:289–300.
- 686 Burt JB, Demirtaş M, Eckner WJ, Navejar NM, Ji JL, Martin WJ, Bernacchia A, Anticevic A, Murray JD.  
687 2018. Hierarchy of transcriptomic specialization across human cortex captured by structural neuroimag-  
688 ing topography. *Nature Neuroscience* **21**:1251–1259. doi:10.1038/s41593-018-0195-0
- 689 Chaplin TA, Yu H-H, Soares JGM, Gattass R, Rosa MGP. 2013. A Conserved Pattern of Differen-  
690 tial Expansion of Cortical Areas in Simian Primates. *Journal of Neuroscience* **33**:15120–15125.  
691 doi:10.1523/JNEUROSCI.2909-13.2013
- 692 Dietrich MR, Ankeny RA, Chen PM. 2014. Publication Trends in Model Organism Research. *Genetics*  
693 **198**:787–794. doi:10.1534/genetics.114.169714
- 694 Dorr AE, Lerch JP, Spring S, Kabani N, Henkelman RM. 2008. High resolution three-dimensional brain  
695 atlas using an average magnetic resonance image of 40 adult C57Bl/6J mice. *NeuroImage* **42**:60–69.  
696 doi:10.1016/j.neuroimage.2008.03.037
- 697 Eichert N, Robinson EC, Bryant KL, Jbabdi S, Jenkinson M, Li L, Krug K, Watkins KE, Mars RB. 2020.  
698 Cross-species cortical alignment identifies different types of anatomical reorganization in the primate  
699 temporal lobe. *eLife* **9**:e53232. doi:10.7554/eLife.53232
- 700 Ellegood J, Anagnostou E, Babineau BA, Crawley JN, Lin L, Genestine M, DiCicco-Bloom E, Lai JK, Y.,  
701 Foster JA, Peñagarikano O, Geschwind DH, Pacey LK, Hampson DR, Laliberté CL, Mills AA, Tam  
702 E, Osborne LR, Kouwer M, Espinosa-Becerra F, Xuan Z, Powell CM, Raznahan A, Robins DM, Nakai  
703 N, Nakatani J, Takumi T, Eede MC van, Kerr TM, Muller C, Blakely RD, Veenstra-VanderWeele J,  
704 Henkelman RM, Lerch JP. 2015. Clustering autism: Using neuroanatomical differences in 26 mouse  
705 models to gain insight into the heterogeneity. *Molecular Psychiatry* **20**:118–125. doi:10.1038/mp.2014.98
- 706 Ellenbroek B, Youn J. 2016. Rodent models in neuroscience research: Is it a rat race? *Disease Models &*  
707 *Mechanisms* **9**:1079–1087. doi:10.1242/dmm.026120
- 708 Englund M, James SS, Bottom R, Huffman KJ, Wilson SP, Krubitzer LA. 2021. Comparing cortex-wide  
709 gene expression patterns between species in a common reference frame. doi:10.1101/2021.07.28.454203
- 710 Fulcher BD, Murray JD, Zerbi V, Wang X-J. 2019. Multimodal gradients across mouse cortex. *Proceedings*  
711 *of the National Academy of Sciences* **116**:4689–4695. doi:10.1073/pnas.1814144116
- 712 Gompers AL, Su-Feher L, Ellegood J, Coping NA, Riyadh MA, Stradleigh TW, Pride MC, Schaffler MD,  
713 Wade AA, Catta-Preta R, Zdilar I, Louis S, Kaushik G, Mannion BJ, Plajzer-Frick I, Afzal V, Visel

- 714 A, Pennacchio LA, Dickel DE, Lerch JP, Crawley JN, Zarbalis KS, Silverman JL, Nord AS. 2017.  
715 Germline Chd8 haploinsufficiency alters brain development in mouse. *Nature Neuroscience* **20**:1062–  
716 1073. doi:10.1038/nrn.4592
- 717 Grzadzinski R, Huerta M, Lord C. 2013. DSM-5 and autism spectrum disorders (ASDs): An opportunity  
718 for identifying ASD subtypes. *Molecular Autism* **4**:12. doi:10.1186/2040-2392-4-12
- 719 Hawrylycz MJ, Lein ES, Guillozet-Bongaarts AL, Shen EH, Ng L, Miller JA, Lagemaat LN van de, Smith  
720 KA, Ebbert A, Riley ZL, Abajian C, Beckmann CF, Bernard A, Bertagnolli D, Boe AF, Cartagena PM,  
721 Chakravarty MM, Chapin M, Chong J, Dalley RA, Daly BD, Dang C, Datta S, Dee N, Dolbeare TA, Faber  
722 V, Feng D, Fowler DR, Goldy J, Gregor BW, Haradon Z, Haynor DR, Hohmann JG, Horvath S, Howard  
723 RE, Jeromin A, Jochim JM, Kinnunen M, Lau C, Lazarz ET, Lee C, Lemon TA, Li L, Li Y, Morris JA,  
724 Overly CC, Parker PD, Parry SE, Reding M, Royall JJ, Schulkin J, Sequeira PA, Slaughterbeck CR, Smith  
725 SC, Sodt AJ, Sunkin SM, Swanson BE, Vawter MP, Williams D, Wohnoutka P, Zielke HR, Geschwind  
726 DH, Hof PR, Smith SM, Koch C, Grant SGN, Jones AR. 2012. An anatomically comprehensive atlas of  
727 the adult human brain transcriptome. *Nature* **489**:391–399. doi:10.1038/nature11405
- 728 Hay M, Thomas DW, Craighead JL, Economides C, Rosenthal J. 2014. Clinical development success rates  
729 for investigational drugs. *Nature Biotechnology* **32**:40–51. doi:10.1038/nbt.2786
- 730 Hedrich HJ, Mossman H, Nicklas W. 2004. Chapter 24: Housing and maintenanceThe Laboratory Mouse.  
731 Elsevier Academic Press. pp. 395–408.
- 732 Heukelum S van, Mars RB, Guthrie M, Buitelaar JK, Beckmann CF, Tiesinga PHE, Vogt BA, Glennon  
733 JC, Havenith MN. 2020. Where is Cingulate Cortex? A Cross-Species View. *Trends in Neurosciences*  
734 **43**:285–299. doi:10.1016/j.tins.2020.03.007
- 735 Hodge RD, Bakken TE, Miller JA, Smith KA, Barkan ER, Graybuck LT, Close JL, Long B, Johansen N,  
736 Penn O, Yao Z, Eggermont J, Höllt T, Levi BP, Shehata SI, Aevermann B, Beller A, Bertagnolli D,  
737 Brouner K, Casper T, Cobbs C, Dalley R, Dee N, Ding S-L, Ellenbogen RG, Fong O, Garren E, Goldy  
738 J, Gwinn RP, Hirschstein D, Keene CD, Keshk M, Ko AL, Lathia K, Mahfouz A, Maltzer Z, McGraw  
739 M, Nguyen TN, Nyhus J, Ojemann JG, Oldre A, Parry S, Reynolds S, Rimorin C, Shapovalova NV,  
740 Somasundaram S, Szafer A, Thomsen ER, Tieu M, Quon G, Scheuermann RH, Yuste R, Sunkin SM,  
741 Lelieveldt B, Feng D, Ng L, Bernard A, Hawrylycz M, Phillips JW, Tasic B, Zeng H, Jones AR, Koch  
742 C, Lein ES. 2019. Conserved cell types with divergent features in human versus mouse cortex. *Nature*  
743 **573**:61–68. doi:10.1038/s41586-019-1506-7
- 744 Horev G, Ellegood J, Lerch JP, Son Y-EE, Muthuswamy L, Vogel H, Krieger AM, Buja A, Henkelman RM,  
745 Wigler M, Mills AA. 2011. Dosage-dependent phenotypes in models of 16p11.2 lesions found in autism.  
746 *Proceedings of the National Academy of Sciences* **108**:17076–17081. doi:10.1073/pnas.1114042108

- 747 Houdebine L-M. 2004. Chapter 6: The mouse as an animal model for human diseasesThe Laboratory Mouse.  
748 Elsevier Academic Press. pp. 97–107.
- 749 Kaas JH. 2012. The evolution of neocortex in primates. *Progress in brain research* **195**:91–102.  
750 doi:10.1016/B978-0-444-53860-4.00005-2
- 751 Kaas JH. 2011a. Reconstructing the Areal Organization of the Neocortex of the First Mammals. *Brain,*  
752 *Behavior and Evolution* **78**:7–21. doi:10.1159/000327316
- 753 Kaas JH. 2011b. Neocortex in early mammals and its subsequent variations. *Annals of the New York*  
754 *Academy of Sciences* **1225**:10.1111/j.1749–6632.2011.05981.x. doi:10.1111/j.1749-6632.2011.05981.x
- 755 Krubitzer L. 2007. The Magnificent Compromise: Cortical Field Evolution in Mammals. *Neuron* **56**:201–  
756 208. doi:10.1016/j.neuron.2007.10.002
- 757 Laubach M, Amarante LM, Swanson K, White SR. 2018. What, If Anything, Is Rodent Prefrontal Cortex?  
758 *eneuro* **5**:ENEURO.0315–18.2018. doi:10.1523/ENEURO.0315-18.2018
- 759 Lein ES, Hawrylycz MJ, Ao N, Ayres M, Bensinger A, Bernard A, Boe AF, Boguski MS, Brockway KS,  
760 Byrnes EJ, Chen L, Chen T-M, Chi Chin M, Chong J, Crook BE, Czaplinska A, Dang CN,  
761 Datta S, Dee NR, Desaki AL, Desta T, Diep E, Dolbeare TA, Donelan MJ, Dong H-W, Dougherty JG,  
762 Duncan BJ, Ebbert AJ, Eichele G, Estin LK, Faber C, Facer BA, Fields R, Fischer SR, Fliss TP, Frenzley  
763 C, Gates SN, Glattfelder KJ, Halverson KR, Hart MR, Hohmann JG, Howell MP, Jeung DP, Johnson  
764 RA, Karr PT, Kawal R, Kidney JM, Knapik RH, Kuan CL, Lake JH, Laramee AR, Larsen KD, Lau C,  
765 Lemon TA, Liang AJ, Liu Y, Luong LT, Michaels J, Morgan JJ, Morgan RJ, Mortrud MT, Mosqueda  
766 NF, Ng LL, Ng R, Orta GJ, Overly CC, Pak TH, Parry SE, Pathak SD, Pearson OC, Puchalski RB,  
767 Riley ZL, Rockett HR, Rowland SA, Royall JJ, Ruiz MJ, Sarno NR, Schaffnit K, Shapovalova NV,  
768 Sivisay T, Slaughterbeck CR, Smith SC, Smith KA, Smith BI, Sodt AJ, Stewart NN, Stumpf K-R,  
769 Sunkin SM, Sutram M, Tam A, Teemer CD, Thaller C, Thompson CL, Varnam LR, Visel A, Whitlock  
770 RM, Wohnoutka PE, Wolkey CK, Wong VY, Wood M, Yaylaoglu MB, Young RC, Youngstrom BL, Feng  
771 Yuan X, Zhang B, Zwingman TA, Jones AR. 2007. Genome-wide atlas of gene expression in the adult  
772 mouse brain. *Nature* **445**:168–176. doi:10.1038/nature05453
- 773 Liu X, Eickhoff SB, Caspers S, Wu J, Genon S, Hoffstaedter F, Mars RB, Sommer IE, Eickhoff CR, Chen  
774 J, Jardri R, Reetz K, Dogan I, Aleman A, Kogler L, Gruber O, Caspers J, Mathys C, Patil KR. 2021.  
775 Functional parcellation of human and macaque striatum reveals human-specific connectivity in the dorsal  
776 caudate. *NeuroImage* **235**:118006. doi:10.1016/j.neuroimage.2021.118006
- 777 Loshchilov I, Hutter F. 2019. Decoupled Weight Decay RegularizationProceedings of the Seventh Interna-  
778 tional Conference on Learning Representations. New Orleans.
- 779 Mandino F, Vrooman RM, Foo HE, Yeow LY, Bolton TAW, Salvan P, Teoh CL, Lee CY, Beauchamp A, Luo

- 780 S, Bi R, Zhang J, Lim GHT, Low N, Sallet J, Gigg J, Lerch JP, Mars RB, Olivo M, Fu Y, Grandjean J.  
781 2021. A triple-network organization for the mouse brain. *Molecular Psychiatry* 1–8. doi:10.1038/s41380-  
782 021-01298-5
- 783 Markello RD, Arnatkeviciūtė A, Poline J-B, Fulcher BD, Fornito A. 2021. Standardizing workflows in  
784 imaging transcriptomics with the abagen toolbox. *Biorxiv* 22.
- 785 Mars RB, Jbabdi S, Rushworth MFS. 2021. A Common Space Approach to Comparative Neuroscience.  
786 *Annual Review of Neuroscience* 44:69–86. doi:10.1146/annurev-neuro-100220-025942
- 787 Mars Rogier B, Passingham RE, Jbabdi S. 2018a. Connectivity Fingerprints: From Areal Descriptions to  
788 Abstract Spaces. *Trends in Cognitive Sciences* 22:1026–1037. doi:10.1016/j.tics.2018.08.009
- 789 Mars RB, Passingham RE, Neubert F-X, Verhagen L, Sallet J. 2016a. Evolutionary specializations of human  
790 association cortexEvolution of Nervous Systems. Academic Press. pp. 185–205.
- 791 Mars RB, Sallet J, Neubert F-X, Rushworth MFS. 2013. Connectivity profiles reveal the relationship between  
792 brain areas for social cognition in human and monkey temporoparietal cortex. *Proceedings of the National  
793 Academy of Sciences* 110:10806–10811. doi:10.1073/pnas.1302956110
- 794 Mars Rogier B, Sotiropoulos SN, Passingham RE, Sallet J, Verhagen L, Khrapitchev AA, Sibson N, Jbabdi S.  
795 2018b. Whole brain comparative anatomy using connectivity blueprints. *eLife* 7. doi:10.7554/eLife.35237
- 796 Mars RB, Verhagen L, Gladwin TE, Neubert F-X, Sallet J, Rushworth MFS. 2016b. Compar-  
797 ing brains by matching connectivity profiles. *Neuroscience & Biobehavioral Reviews* 60:90–97.  
798 doi:10.1016/j.neubiorev.2015.10.008
- 799 Myers E. 2017. Molecular neuroanatomy: Mouse-human homologies and the landscape of genes implicated  
800 in language disorders (PhD thesis). Boston University.
- 801 NCBI. 2018. Database resources of the National Center for Biotechnology Information. *Nucleic Acids  
802 Research* 46:D8–D13. doi:10.1093/nar/gkx1095
- 803 Neubert F-X, Mars RB, Thomas AG, Sallet J, Rushworth MFS. 2014. Comparison of Human Ventral  
804 Frontal Cortex Areas for Cognitive Control and Language with Areas in Monkey Frontal Cortex. *Neuron*  
805 81:700–713. doi:10.1016/j.neuron.2013.11.012
- 806 Oh SW, Harris JA, Ng L, Winslow B, Cain N, Mihalas S, Wang Q, Lau C, Kuan L, Henry AM, Mortrud MT,  
807 Ouellette B, Nguyen TN, Sorensen SA, Slaughterbeck CR, Wakeman W, Li Y, Feng D, Ho A, Nicholas  
808 E, Hirokawa KE, Bohn P, Joines KM, Peng H, Hawrylycz MJ, Phillips JW, Hohmann JG, Wohnoutka  
809 P, Gerfen CR, Koch C, Bernard A, Dang C, Jones AR, Zeng H. 2014. A mesoscale connectome of the  
810 mouse brain. *Nature* 508:207–214. doi:10.1038/nature13186
- 811 Ortiz C, Fernandez Navarro J, Jurek A, Martin A, Lundeberg J, Meletis K. 2020. Molecular atlas of the  
812 adult mouse brain. *Science Advances* 6:14.

- 813 Pagani M, Barsotti N, Bertero A, Trakoshis S, Ulysse L, Locarno A, Miseviciute I, De Felice A, Canella C,  
814 Supekar K, Galbusera A, Menon V, Tonini R, Deco G, Lombardo MV, Pasqualetti M, Gozzi A. 2021.  
815 mTOR-related synaptic pathology causes autism spectrum disorder-associated functional hyperconnec-  
816 tivity. *Nature Communications* **12**:6084. doi:10.1038/s41467-021-26131-z
- 817 Passingham RE, Stephan KE, Kötter R. 2002. The anatomical basis of functional localization in the cortex.  
818 *Nature Reviews Neuroscience* **3**:606–616. doi:10.1038/nrn893
- 819 Preuss TM. 1995. Do rats have prefrontal cortex? The Rose-Woolsey-Akert program reconsidered. *Journal  
820 of Cognitive Neuroscience* **7**:24.
- 821 Qiu LR, Fernandes DJ, Szulc-Lerch KU, Dazai J, Nieman BJ, Turnbull DH, Foster JA, Palmert MR, Lerch  
822 JP. 2018. Mouse MRI shows brain areas relatively larger in males emerge before those larger in females.  
823 *Nature Communications* **9**:2615. doi:10.1038/s41467-018-04921-2
- 824 Richards K, Watson C, Buckley RF, Kurniawan ND, Yang Z, Keller MD, Beare R, Bartlett PF, Egan  
825 GF, Galloway GJ, Paxinos G, Petrou S, Reutens DC. 2011. Segmentation of the mouse hippocampal  
826 formation in magnetic resonance images. *NeuroImage* **58**:732–740. doi:10.1016/j.neuroimage.2011.06.025
- 827 Rudebeck PH, Izquierdo A. 2022. Foraging with the frontal cortex: A cross-species evaluation of reward-  
828 guided behavior. *Neuropsychopharmacology* **47**:134–146. doi:10.1038/s41386-021-01140-0
- 829 Sallet J, Mars RB, Noonan MP, Neubert F-X, Jbabdi S, O'Reilly JX, Filippini N, Thomas AG, Rushworth  
830 MF. 2013. The Organization of Dorsal Frontal Cortex in Humans and Macaques. *Journal of Neuroscience*  
831 **33**:12255–12274. doi:10.1523/JNEUROSCI.5108-12.2013
- 832 Schaeffer DJ, Hori Y, Gilbert KM, Gati JS, Menon RS, Everling S. 2020. Divergence of rodent and pri-  
833 mate medial frontal cortex functional connectivity. *Proceedings of the National Academy of Sciences*  
834 **117**:21681–21689. doi:10.1073/pnas.2003181117
- 835 Simonoff E, Pickles A, Charman T, Chandler S, Loucas T, Baird G. 2008. Psychiatric Disorders in Children  
836 With Autism Spectrum Disorders: Prevalence, Comorbidity, and Associated Factors in a Population-  
837 Derived Sample. *Journal of the American Academy of Child & Adolescent Psychiatry* **47**:921–929.  
838 doi:10.1097/CHI.0b013e318179964f
- 839 Stahl PL, Salmén F, Vickovic S, Lundmark A, Navarro JF, Magnusson J, Giacomello S, Asp M, Westholm  
840 JO, Huss M, Mollbrink A, Linnarsson S, Codeluppi S, Borg Å, Pontén F, Costea PI, Sahlén P, Mulder  
841 J, Bergmann O, Lundeberg J, Frisén J. 2016. Visualization and analysis of gene expression in tissue  
842 sections by spatial transcriptomics. *Science* **353**:78–82. doi:10.1126/science.aaf2403
- 843 Steadman PE, Ellegood J, Szulc KU, Turnbull DH, Joyner AL, Henkelman RM, Lerch JP. 2014. Genetic  
844 Effects on Cerebellar Structure Across Mouse Models of Autism Using a Magnetic Resonance Imaging  
845 Atlas: MRI of genetic mouse model's cerebellum. *Autism Research* **7**:124–137. doi:10.1002/aur.1344

- 846 Striedter GF, Northcutt RG. 2020. Brains Through Time. Oxford University Press.
- 847 Sundararajan M, Taly A, Yan Q. 2017. Axiomatic Attribution for Deep NetworksProceedings of the 34th  
848 International Conference on Machine Learning. PMLR. pp. 3319–3328.
- 849 Ullmann JFP, Watson C, Janke AL, Kurniawan ND, Reutens DC. 2013. A segmentation protocol and MRI  
850 atlas of the C57BL/6J mouse neocortex. *NeuroImage* **78**:196–203. doi:10.1016/j.neuroimage.2013.04.008
- 851 Ventura-Antunes L, Mota B, Herculano-Houzel S. 2013. Different scaling of white matter volume, cor-  
852 tical connectivity, and gyration across rodent and primate brains. *Frontiers in Neuroanatomy* **7**.  
853 doi:10.3389/fnana.2013.00003
- 854 Vickovic S, Eraslan G, Salmén F, Klughammer J, Stenbeck L, Schapiro D, Äijö T, Bonneau R, Bergenstråhl  
855 L, Navarro JF, Gould J, Griffin GK, Borg Å, Ronaghi M, Frisén J, Lundeberg J, Regev A, Ståhl PL.  
856 2019. High-definition spatial transcriptomics for *in situ* tissue profiling. *Nature methods* **16**:987–990.  
857 doi:10.1038/s41592-019-0548-y
- 858 Wang Q, Ding S-L, Li Y, Royall J, Feng D, Lesnar P, Graddis N, Naeemi M, Facer B, Ho A, Dolbeare T,  
859 Blanchard B, Dee N, Wakeman W, Hirokawa KE, Szafer A, Sunkin SM, Oh SW, Bernard A, Phillips  
860 JW, Hawrylycz M, Koch C, Zeng H, Harris JA, Ng L. 2020. The Allen Mouse Brain Common Coordinate  
861 Framework: A 3D Reference Atlas. *Cell* **181**:936–953.e20. doi:10.1016/j.cell.2020.04.007
- 862 Yao Z, Velthoven CTJ van, Nguyen TN, Goldy J, Sedeno-Cortes AE, Baftizadeh F, Bertagnoli D, Casper  
863 T, Chiang M, Crichton K, Ding S-L, Fong O, Garren E, Glandon A, Gouwens NW, Gray J, Graybuck  
864 LT, Hawrylycz MJ, Hirschstein D, Kroll M, Lathia K, Lee C, Levi B, McMillen D, Mok S, Pham T,  
865 Ren Q, Rimorin C, Shapovalova N, Sulc J, Sunkin SM, Tieu M, Torkelson A, Tung H, Ward K, Dee N,  
866 Smith KA, Tasic B, Zeng H. 2021. A taxonomy of transcriptomic cell types across the isocortex and  
867 hippocampal formation. *Cell* **184**:3222–3241.e26. doi:10.1016/j.cell.2021.04.021

868 **Figure supplements**

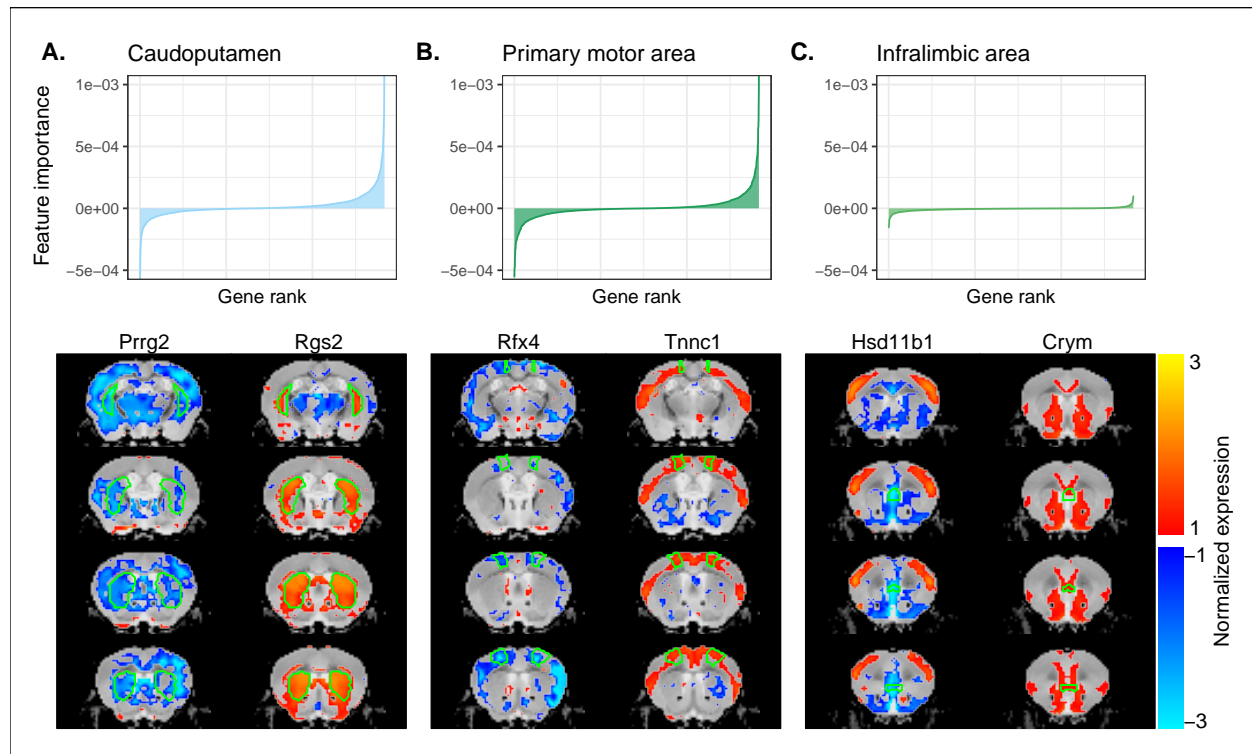


**Figure 2-figure supplement 1.** Multi-layer perceptron feature importance.